PREC
PUERTO RICO ENERGY CENTER

SUMMER INTERNSHIP 2017

CLEAN TECHNOLOGIES RESEARCH

Volume 5

CIESESE
Consortium for Integrating Energy Systems in Engineering & Science Education
DE-NA0003330

DEPARTMENT OF ENERGY
UNITED STATES OF AMERICA
DE-NA0003330

Editors

Silvia Casillas

Suheilie Rodríguez

Armando Soto

José G. Maeso

This material is based upon work supported by the Department of Energy/National Nuclear Security Administration under Award Number(s) DE-NA0003330

The PREC Summer Internship began in 2010 as a tool to provide a research experience to college students, as part of the efforts of US DoE Massie Chair of Excellent Grant (DE-NA0000672) and Universidad del Turabo Puerto Rico Energy Center. This experience included working on a research project, writing a scientific paper and preparing and providing a technical presentation to their peers. Students also participate in technical workshop that have raged from literature review techniques to mentoring. For most of the participating students this was their first experience doing research and has served them to pursue careers in research in the academia, private sector and government. Their scientific work has allowed our student to deepen in research subject and publish in peer reviews journals and proceedings. Approximately 50 mentors and 140 students have benefited from the program, and through years the quality and diversification of the participating projects have been remarkable. It is our goal to continue providing successful research experiences to undergraduates and graduate students as well as to improve the research capabilities and products of the Universidad del Turabo and Puerto Rico.

Roberto Lorán Santos, PhD

Principal Investigator

Consortium for Integrating Energy System in Engineering and Science Education (CIESESE)

DE-NA0003330

Amaury J. Malavé Sanabria, PhD

Executive Director PREC

Consortium for Integrating Energy System in Engineering and Science Education (CIESESE)

DE-NA0003330

Preface

1 Biofuels From Microalgae: Development of a Rapid Method for Screening High Lipid Containing Species

4 Control Design of a Micro-Wind Turbine System Application

9 Low energy consumption real-time tracker

13 Optimal Wind Tunnel for Testing Small Scale Wind Turbines

15 PV solar panel orientation for load following

19 Waste materials from land fields and wetlands as energy source: Nitrogen profile of an urban wetland

21 Vertical Axis Wind Turbine Generator

27 Use of Vegetation for Energy Efficiency Improvement

34 Bacterial Bioprospecting for Bioenergy Applications: Xylose Fermentation

38 Growing Chlorella sorokiniana heterotrophically, with sodium bicarbonate as a source of carbon

Contents

Biofuels From Microalgae: Development of a Rapid Method for Screening High Lipid Containing Species

Paulette González Lamenza[1], Harim Delgado Seo[2], Catalina Dávila Aguer[3]
Department of Biology, School of Natural Science and Technology at Universidad del Turabo, Gurabo, Puerto Rico
pgonzalez@email.suagm.edu[1], hdelgado28@email.suagm.edu[2], davilac2@suagm.edu[3]

***Abstract*—Investigators from various fields of study have moved away from searching for an alternative biofuel in crops such as soybeans and corn that could replace the current use of fossil fuels, because of their slow production rate. Instead, a new wave of scientists has identified the potential and benefits that microalgae have over those crops. On the other hand, the cultivation of microalgae also has its own complications that need to be managed before mass production. When searching for promising species, one of the difficulties encountered is the lack of a rapid tactic to determine the neutral lipid content in microalgae. Traditionally, lipid content assessment has been examined by the gravimetric method, which is cost and labor intensive and time consuming. Nile red staining has proved to help in the quantification of intracellular lipid bodies in microalgae and several protocols have been developed. However, most of these protocols work with a limited number of species and a suitable staining methodology has been difficult to develop with thick cell wall species. We aimed to develop a protocol for staining lipids in Botryococcus sudeticus, a thick cell wall microalga, involving Nile red addition coupled with cell wall break. Three different procedures were examined and compared with the traditional Nile red staining method, as described previously.**

***Keywords*—microalgae;Botyococcus Sudeticus; biofuel; neutral lipids; fluorescence; Nile red; DMSO**

I. Resumen

Investigadores de diversos campos de estudio se han alejado de biocombustibles alternativos a base de plantas tales como la soja y el maíz que podrían reemplazar el uso actual de combustibles fósiles, debido a su baja tasa de producción. Una nueva ola de científicos ha identificado el potencial y los beneficios que las microalgas tienen sobre estos cultivos. Por otra parte, el cultivo de microalgas también tiene sus propias complicaciones que necesitan ser manejadas antes de la producción en masa. En la búsqueda de especies prometedoras, una de las dificultades encontradas es la falta de una táctica rápida para determinar el contenido de lípidos neutros en las microalgas. Tradicionalmente, la evaluación del contenido de lípidos se ha examinado por el método gravimétrico, que es costoso y requiere mucho trabajo y tiempo. La tinción con Nilo rojo ha demostrado ser de ayuda en la cuantificación de cuerpos lipídicos intracelulares en microalgas y varios protocolos han sido desarrollados. Sin embargo, la mayoría de estos protocolos trabajan con un número limitado de especies y ha sido difícil desarrollar una metodología de tinción adecuada con especies de pared celular gruesa. Nuestro objetivo fue desarrollar un protocolo para la tinción de lípidos en Botryococcus sudeticus, una microalga con una pared celular gruesa. Este protocolo incluyó la adición de Nilo rojo y el rompimiento de la pared celular. Se examinaron tres procedimientos diferentes y se compararon con el método tradicional de tinción con Nilo Rojo, descrito anteriormente

II. Introduction

As the exhaustion of fossil fuels and the worry over global warming increases over time, so has the search for a viable fossil fuel replacement. Most candidates fall under the category of biofuels. In fact, the most well-known example of a biofuel would be the biodiesel, commercially produced through lipid transesterification of plant derivatives. In the past decade, studies with microalgae as a primary source of oil, have increased in the effort to bring forward a viable feedstock for a large-scale production of biodiesel. Contrary to biodiesel producing terrestrial plant harvests, one of the major benefits that microalgae have over crops is that they produce 30 times more biodiesel-convertible lipid content (up to 60% of biomass) per 10,000 m2 than crop fields of an equal size [1].

Another disadvantage of the cultivation of biodiesel crop is the competition over agricultural lands with the food industry. The production of biodiesel derived from microalgae lacks the necessity to occupy arable or agricultural land, since a vast number of microalgae come from and can be harvested in seawater and wastewater [2]. Consequently, the production of microalgae does not impose competition for agricultural lands, or occupy essential life-sustaining habitats such as fresh water resources. It is also important to mention that, as photosynthetic organisms, microalgae can assimilate carbon dioxide efficiently and have been proposed as a suction or pollution processor for discharged carbon dioxide and other gaseous pollutants in the atmosphere. In other words, microalgae counteract the release of greenhouse gases by recycling them. Therefore, they reduce the ecological imprint left on the environment. Furthermore, they have recently played a major role as a bioremediation tool when cultivated in phosphorus and nitrogen rich wastewaters [1]. As a result, many effluents have benefited by their cultivation.

As mentioned above, the cultivation of microalgae to produce biodiesel does provide multiple useful remedies for other ecological problems. However, there are also some financial and technical obstacles that need to be overcomed before being introduced in the market [2]. To make biodiesel production feasible from microalgae, investigators need to identify species exhibiting high lipid content potential and rapid growth patterns. Hence, a successful method of quantitative lipid measurement needs to be elaborated and serve as a diagnostic tool for collected specimens of microalgae and dictate from their results whether their production would be a success or not. [3].

The traditional method for quantifying the lipid content of microalgae consists of extracting the lipids from the microalgae and measuring them gravimetrically [3]. However, it requires and consumes a large amount of time, money and labor. In contrast, the Nile red method is a simpler alternate method of measurement that involves less labor-intensive work. Past experiences have proven that this method is a reliable one for certain species, but most of the green algal species have a thicker cell wall that does not permit the proper diffusion of the Nile red dye into the intercellular lipid bodies, making the method less consistent for certain specimens. To resolve the experiment's inconclusive outcomes, we included additional steps for a new protocol to help the infusion of the hydrophobic Nile red molecules into the cytoplasm and further the rupture of the cell walls with the addition of dimethyl sulfoxide (DMSO), and the use of household microwaves and vortexes.

For the Nile red method, factors such as temperature, staining time, and concentration of DMSO need to be optimized for enhanced results. The aim of this study was to design a protocol that could effectively stain the lipid content found in both thin and thick celled microalgae species, so that one protocol could be used among all specimens without the need to make significant changes or adjustments to the procedure [6].

III. METHODOLOGY

Four different protocols with microwave and DMSO-assisted steps were designed to ensure effectivity and determine the presence of neutral lipids while assessing their quantity [6].

A. Materials

A Nile red stock solution and an algal strain of *Botryococcus sudeticus* were used during the experiments and both remained fixed variables on all four experiments. Additional materials were DMSO, a vortex and a household microwave.

B. Methods

1) Fixed variables

a) Cultivation: The Botryococcus sudeticus living algal strain was obtained commercially from UTEX Culture Collection of Algae and it is identified as UTEX B2629. It was inoculated in Soil Extract medium and incubated under constant light and agitation at room temperature.

b) DMSO concentration: The DMSO concentration was left at 20%, stated in reference [4] as the optimal concentration for best results, and aliquots of 5 mL were introduced in the centrifuge tube with the inoculum when required.

c) Nile red concentration: Aliquots of 75 µL were introduced in the centrifuge tube with the inoculum two times when required.

d) Staining time and temperature: The standard time for optimal results were 15 minutes at a temperature of 37 ºC in Experiment A and C (see below) and room temperature in the other experiments; all in total obscurity. Said conditions were achieved by means of an bacterial incubator.

2) Protocols: The experiment was divided into four different experimental protocols, to verify and eliminate ineffective steps or procedures. Each of the four experiments had two replicates and the assigned control groups were the algal sample (without DMSO or the Nile red solution), and the Nile Red solution alone. Figure 1 shows the general protocol followed to stain microalgal lipids.

1. Introduce 5 ml of algal sample into a centrifuge tube.
2. Centrifuge at 8,000 g / 10 minutes at room temperature.
3. Wash pellet with distilled water three times before adding 10 ml of DMSO or distilled water depending on the experiment being carried.
4. Leave in sonic bath for 10 minutes.
5. Microwave for 30 seconds with 2-3 intervals of a few seconds, if the experiment requires it.
6. Introduce 75 µl of Nile red stock solution.
7. Microwave again using the previous technique, if the experiment requires it.
8. Use vortex on samples for 1 minute.
9. Leave samples in an incubator in total obscurity for 15 minutes.
10. Transfer samples to the fluorimeter cuvette for analysis.

Fig. 1 Generic protocol for staining intracellular lipid bodies

a) Experiment A: Microwave assisted experiment with DMSO. Five mililiters of algal sample were centrifuged at 8,000 g / 10 minutes at room temperature. The pellet was washed with distilled water three times. Ten mililiters of DMSO were added and the mixture was left in a sonicator bath for 10 minutes to facilitate cell disruption. Then, the samples were microwaved for 30 seconds with 2-3 intervals of 8 to 10 seconds to allow the sample to cool down and prevent it from spilling out. An aliquote of 75 µL of Nile red was added, and incubated for 10 minutes at 37 ºC in darkness. It was microwaved again using the same technique. Samples were vortexed for 1 minute and left at 25 ºC in the dark for 15 minutes.

b) Experiment B: Non-microwave assisted experiment with no DMSO. Five mililiters of the algal culture were centrifuged at 8,000 g / 10 minutes at room temperature. The pellet was washed with distilled water three times. Ten mililiters of distilled water were added and the mixture was left in a sonicator bath for 10 minutes. Then, 75 µL of Nile red were added. Samples were vortexed for 1 minute and left at 25 ºC in the dark for 15 minutes.

c) Experiment C: Non-microwave assisted experiment with DMSO. Five mililiters of the algal culture were centrifuged at 8,000 g / 10 minutes at room temperature. The pellet was washed with distilled water three times. Ten mililiters of DMSO were added and the mixture was left in a sonicator bath for 10 minutes. Then, 75 µL of Nile red were added. Samples were vortexed for 1 minute and left at 25 ºC in the dark for 15 minutes.

d) Experiment D: Microwave assisted experiment with no DMSO. Five mililiters of the algal culture were centrifuged at 8,000 g / 10 minutes at room temperature. The pellet was washed with distilled water three times. Ten mililiters of distilled water were added and the mixture was left in a sonicator bath for 10 minutes. Then, the samples were microwaved for 30 seconds with intervals. An aliquote of 75µL of Nile red was added and incubated for 10 minutes at 37ºC, then microwaved again using the same technique. Samples were vortexed for 1 minute and left at 25 ºC in the dark for 15 minutes.

After the formerly listed protocols were conducted, the samples were taken and transferred into a cuvette for fluorescence analysis. The excitation and emission wavelengths established settings were set at 530 nm and 368 nm [5].

IV. Results

Polar lipids could not be detected, indicating that under the culture conditions employed in this study, B. sudeticus did not accumulate lipids, even after 14 days of incubation, when the algae was reaching the stationary phase of growth. Thus, the protocols developed could not be tested. However, we observed differences in the emission of chlorophyll which indicated distinct cell disruption levels in each protocol. As seen in Table 1, the emission of chlorophyll was higher in the culture treated with DMSO and microwave, followed by the culture treated only with DMSO. The sample treated only with microwaves resulted in a lower emission spectra when compared to the control (no microwaves nor DMSO). This could mean that the microwave treatment did not increase the permeability of the cell wall enough and possibly should not be included as a strategy to aid in NR staining. These experiments will be repeated with several microalgal strains in order to validate these results.

TABLE I. RESULTS FROM FLUOROMETRIC ANALYSIS

Sample	Emission Fluorescence
Algal culture stained with traditional method	38.46
Algal culture treated with DMSO + Microwave	54.179
Algal culture treated with DMSO	52.6765
Algal culture treated with microwave	29.8065
Non stained culture	74.929
Nile red	267.342

Acknowledgments

As this project would have not been possible without their guidance, we would like to give a special thanks to the PREC personnel for allowing us to participate in the Summer Internship Program of 2017. We also thank Dr. Catalina Dávila for providing us with the fortunate experience of working with microalgae, one of the first times in Puerto Rico. Her exemplary guidance helped us as newcomers to understand the workings that undergo the research environment. Additional honorable mentions should go to Olga García, Shakira Martínez, Luis Álvarez, Nathalia Pérez, and Nicole Silva, other undergraduate researchers who equally contributed to the same project along us.

During the internship, we also received further guidance, advice and knowledge from professionals from a variety of scientific disciplines by means of seminars. We would like to thank Dr. José R. Pérez Jiménez for arranging those seminars and giving orientation to us. The contribution of those professionals greatly enhanced our learning experience and performance during the experimentation process.

References

[1] J. M. Graham, L.E. Graham, S. B. Zulkifly, B. F. Pfleger, S. W. Hoover and J. Yoshitani, Fresh diatoms as a source of lipids for biofuels, *Journal of Industrial Microbiology*, vol. 39, pp. 419-428, March 2012.

[2] M. M. Loera-Quezada and E. J. Olgín, Las microalgas oleaginosas como fuente de biodiesel: retos y oportunidades, *Rev. Latinoam. Biotechnol. Amb. Algal*, vol. 1, pp. 91-116, 2010.

[3] M. M. Loera-Quezada and E. J. Olgín, Oil microalgae as a source of biodiesel: challenges and opportunities, *Rev. Latinoam. Biotechnol. Amb. Algal*, vol. 1, pp. 91-116, 2010.

[4] R. Halim and P. A. Webley, Nile Red Staining for Oil Determination in Microalgal Cells: A New Insight through Statistical Modelling, *International Journal of Chemical Engineering*, vol of 2015, Article ID 695061, pp. , 2015.

[5] W. Chen, C. Zhang, L. Song, M. Sommerfeld and Q. Hu, A high throughtout Nile red method for quantitative measurement of neutral lipids in microalgae, *Journal of Microbiological Methods*, vol. 77, pp. 41-47, 2009.

[6] G. Huang, G. Chen and F. Chen, Rapid screening method for lipid production in alga based on Nile red fluorescence, *Biomass and Bioenergy*, vol. 33, pp. 1386-1392, 2009.

[7] W. Chen, W. Sommerfeld and Q. Hu, Microwave-assisted Nile red method for in-vivo quantification of neutral lipids in microalgae, *Bioresource Technology*, vol. 102, pp. 135-141, 2011.

[8] D. Elsay, D. Jameson, B. Raleigh, & M. J.Cooney, Fluorescent measurement of microalgal neutral lipid. *Journal of Microbiological Methods*, vol. 68, pp. 639-642, August 2006.

Control Design of a Micro-Wind Turbine System Application

Luis Benítez-Montalván[1], Juan Rivera-Cruz[2], Diego Aponte-Roa[3]
Department of Electrical and Computer Engineering, School of Engineering at University of Turabo,
Gurabo Puerto Rico lbenitez25@email.suagm.edu[1], jrivera1118@email.suagm.edu[2], aponted1@suagm.edu[3]

***Abstract*—Wind energy can be considered a consolidated renewable source to produce electrical energy due to its advances in recent decades for practical applications. This explains why every day micro-wind turbines are becoming more popular and emerging as one of the most promising technologies in the field of energy systems. Due to the natural behavior of wind turbines, recent research is focused on the design of a control system to optimize the power production and operate the turbine with safety. This paper presents the implementation of a buck-boost DC-DC converter to either step-up or step-down the voltage supplied by a wind generator to a constant load of 10W. Matlab was used to model the complete system. A comparison between simulation and premilinar experimental results is presented as well.**

***Keywords*—Buck-Boost Converter; Rectifier; Infrared; Capacitor Bank**

I. Introduction

Wind energy has long served as a power source to humans for years. Historically, cities around Sri Lanka used the monsoon winds to power furnaces as early as 300 BCE [1]. Today, the use of wind turbines for generating electricity has become a popular renewable energy choice over the past years, although new investment in clean energy fell to 287.5bn, 18% lower than the record of 348.5bn in 2015. Offshore wind was the brightest spot in 2016, with commitments of 29bn in 2016 which is 40% more than the previous year [2].

Over the past decade wind turbine use has increased more than 25% per year. Still, it only provides a small fraction of the world’s energy needs. From 2001 to 2016, cumulative wind capacity around the world increased from 23,900 megawatts to more than 486,000 megawatts [3]. According to the World Energy Outlook of 2016 the wind generated electricity met close to 4% of the world’s electricity demand in 2015, which is a record-setting year with more than 63 GW of new wind power capacity installed. The global wind energy potential is vast: wind energy could account for up to 30% of global power generation by 2040 [4].

Recent research is focused on micro-wind turbines to power small electrical devices such as LED signs, cell phone batteries, and other devices of low power. The power output of micro-wind turbines is much less than small-scale and large-scale wind turbines, but represents a form of low cost energy generation for specific applications such as lighting up the streets on urban or isolated places. These types of turbines are generally characterized as micro-scale turbines and designed to work under low wind speeds (3-15 m/s approx.) [5].

One big challenge of wind power is the fact that the wind is unpredictable even at the best wind places, those with steady reasonable high-wind speed wind. There are variations in speed and direction of the wind which affect the ability of the wind turbine to deliver power. Larger wind turbine systems have complex control systems which automatically track changes in wind direction and speed, and adjust turbine orientation, blade pitch, and generator gearing to maintain the desired electrical output. Micro-wind turbine systems are typically much less sophisticated; however, they generally still have some form of control to improve their longevity and power production [6]. The main purpose of the control system is to protect the turbine and generator from over-speeding, as well as optimizing the power production.

II. Experimental Procedure

A. Three-Phase Rectifier

A three-phase rectifier was placed at the output of the generator in order to convert the AC voltage produced by the generator to DC voltage that is directly connected to a system of power electronics.

The rectifier consists on a set of two diodes, each connected to one phase. The system will completely rectify both the positive and negative half cycles, producing six pulses of output voltage. Schottky diodes were used to prevent a significant voltage drop. Also, a capacitor bank was connected across the output terminals of the rectifier to stabilize and eliminate the ripple effect of the output DC signal (see Fig. 1).

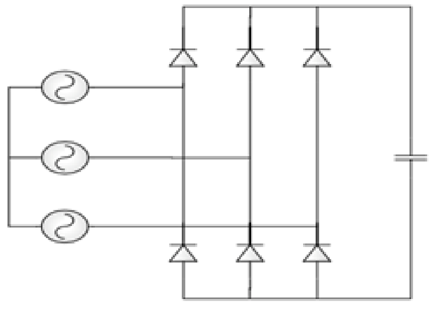

Figure 1. Three-Phase Rectifier

To test this type of rectifier, the laboratory of electric machines was used. Such laboratory includes modern equipment to produce both monophasic and polyphasic AC voltage sources, where the magnitude can be adjusted. To measure all three phases and the DC output signal, a 4-channel oscilloscope was used. An estimation of the DC output voltage can be estimated by using the following equation:

$$Vdc = \frac{3\sqrt{3}}{\pi} Vpeak$$

B. *Pulse-Width Modulation (PWM)*

To turn on and off the N-Channel MOSFET transistor that is used as a digital switch in the power electronics system, a square wave signal with a desired duty cycle and frequency was created using a microcontroller (MCU). Figure 2 shows an example.

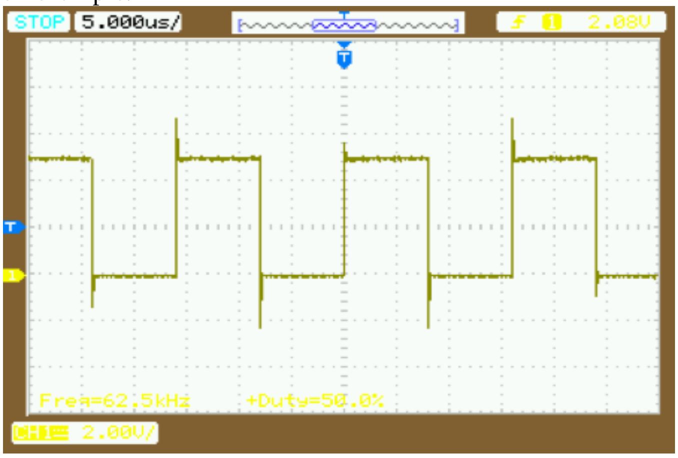

Figure 2. Squared signal at 62.5KHz with 50% of duty cycle

C. *Power Electronics System*

In order to maximize the power produced by the wind turbine and operate a 10W led light used as the load, a buck-boost converter (see Fig. 3) was used, in which the output voltage can be less, greater, or even equal to the input voltage.

✓ On-State

When the power MOSFET is on, the current in the inductor will increase linearly with time. The diode will be in reversed-biased mode and blocking the current flow from the voltage source, while the capacitor is delivering the energy previously stored to the load.

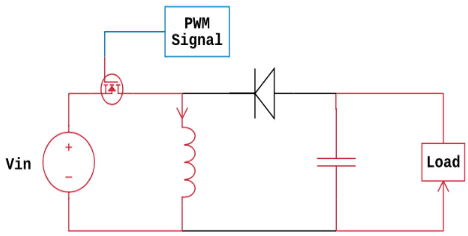

Figure 3. Buck-Boost Converter during On-State

✓ Off-State

When the power MOSFET is off, the voltage in the inductor is reversed and the diode will be in forward region, thus conducting current. The current previously stored in the inductor will be delivered to both the capacitor and the load.

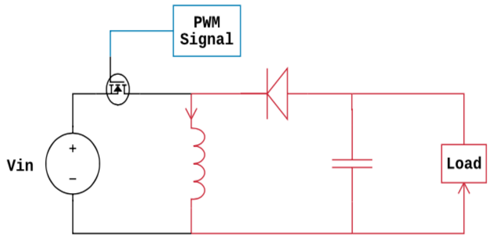

Figure 4. Buck-Boost Converter during Off-State

The gain of the output voltage depends on the duty cycle of the signal, for instance if the duty cycle is less than 50%, then the output voltage is less than the input voltage; otherwise, the output voltage will be greater than the input voltage. The following equation is used to determine the output voltage:

$$Vout = \frac{D}{1-D} Vin$$

where: D= % Duty Cycle

D. *Embedded System*

To operate the wind turbine at safety levels and constantly monitor measurements like voltage, current, angular velocity, and power, an MCU had to be used along with the integration of a variety of sensors.

Two voltage sensors were implemented to measure both the input and output voltage while an infrared sensor was used to measure the angular velocity. On the other hand, a current sensor based on the Hall effect was implemented to convert the current to a voltage signal.

E. *Brake System*

For this part, three two-state relay modules were used in order to route the power generated between the rectifier and a braking resistive load. In the case the generator doesn't exceed the maximum ratings of angular velocity, then the relays route the power directly to the power electronics system. Otherwise, the power generated is routed to a resistive load with low resistance and high wattage rating.

The low-ohm resistor allows a large amount of current to return back into the generator stator, thereby increasing the electrical torque to counteract the mechanical torque of the turbine to achieve equilibrium in the system. See figure 5 for the connection diagram.

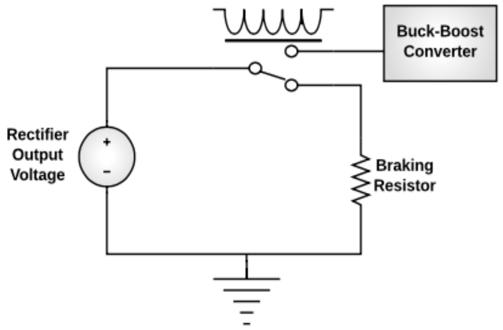

Figure 5. Braking System Connection

F. Complete System Design and System Modeling

A complete system design diagram is presented in Figure 6.

To predict and analyze the behavior of some of the subsystems like the rectifier and the DC-DC converter, MATLAB/Simulink software was used, along with the power-electronics library.

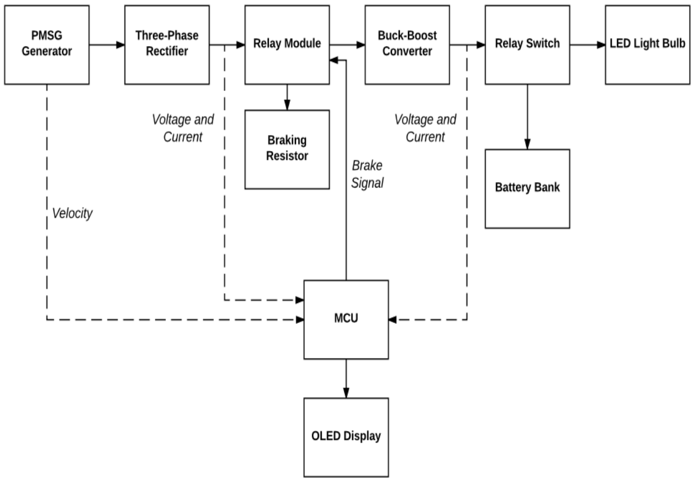

Figure 6. System Design Diagram

The first model made was the three-phase rectifier (see Fig. 7), where the parameters of each component had to be adjusted to comply with the electrical characteristics. Some of those parameters were the forward voltage of the diode, diode resistance, and frequency of the AC sources.

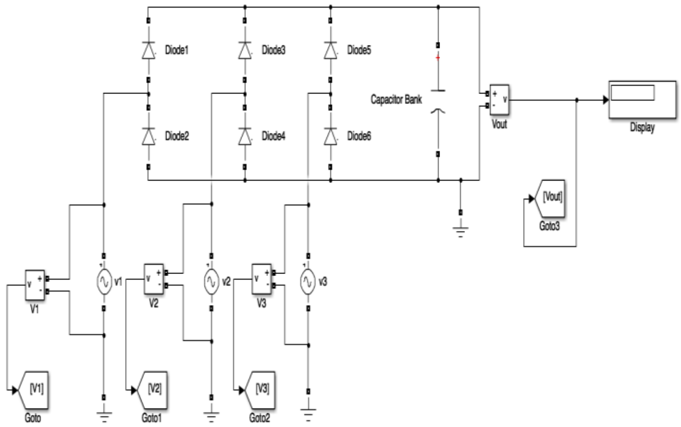

Figure 7. Three-Phase Rectifier Model

Figure 8 shows the model of a buck-boost converter implemented as well.

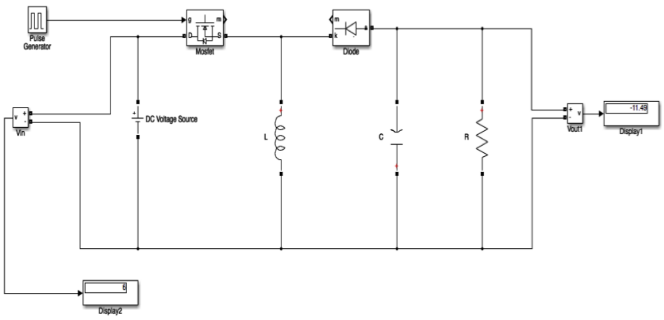

Figure 8. Buck-Boost Converter Model

III. Results

Figure 9 shows the results for the simulation of the three-phase rectifier. The yellow, violet, and red graphs represent the three phases of the voltage source, each 120º out of phase while the green signal represents the output DC signal with low ripple effect due to the high capacitance that is connected in parallel across the output terminals of the rectifier.

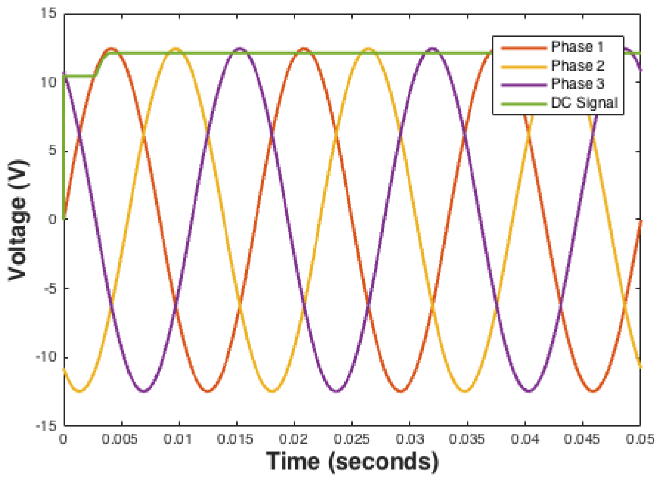

Figure 9. Rectifier Simulation Results

Figure 10 represents experimental results that were collected in the electric machines laboratory.

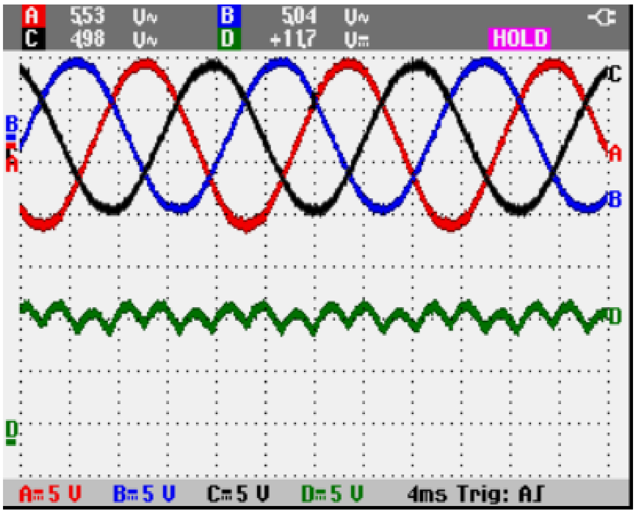

Figure 10. Rectifier Experimental Results

Table 1 shows the results obtained in the simulation of the buck-boost converter. The results show a testing for two different input voltages, where the DC-DC converter acts as a buck and boost converter according to the percentage of the duty cycle.

Table I. DC-DC Converter Simulation Results

Vin	% Duty Cycle	Vout
6V	45%	4.61V
6V	55%	7.03V
12V	45%	9.52V
12V	55%	14.36V

Figure 11 shows a graph of the efficiency of the buck-boost converter used in the assembled circuit. The maximum efficiency of the converter was obtained at 10V. Input voltages that are outside the range of 10V-15V decrease significantly the system efficiency.

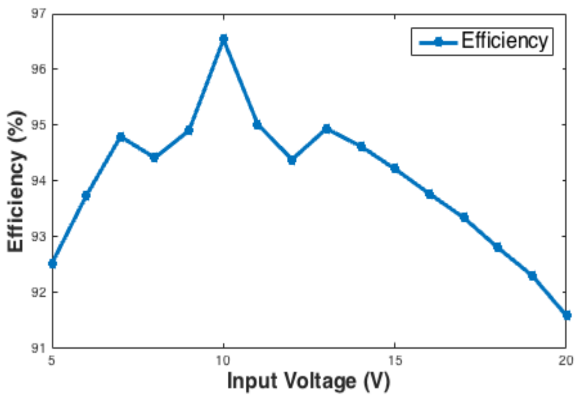

Figure 11. Efficiency of the Converter

Figure 12 shows the assembled circuit for the control system.

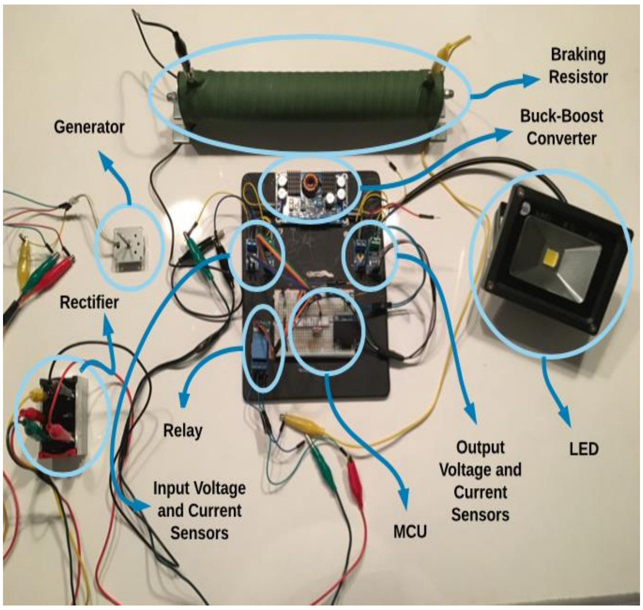

Figure 12. Assembled Circuit

The complete system was very stable and capable of delivering the necessary power to the 10W led light (load).

The load at maximum power dissipated provide 900 lumens of light intensity. This type of illumination intensity is useful for outdoor and indoor lighting projects, for gardens, garages, warehouses, and show windows. The relay module was responding to the digital signals coming from the MCU, however, a bigger generator in motion needs to be connected to the relay module to verify if the electrical torque is sufficient to counteract the mechanical torque and achieve full system equilibrium.

IV. Conclusion

A wind turbine is a sustainable source of renewable energy, but due to the unpredictable behavior of environmental factors a stable control system needs to be implemented to keep it safe and extract the maximum power out of the generator by implementing a high efficiency power electronics system. Our control system include a MCU to manage all sensors to display accurate readings of voltage, current, and power consumptions of the whole system. Preliminar results shows an efficiency from 91.5% to 96.5% for different expected input voltages supplying a constant load of 10W. Future work includes adding a battery bank to store the energy produced in excess.

Acknowledgment

Authors acknowledge both the Puerto Rico Energy Center (PREC) and the Consortium for Integrating Energy Systems in Engineering and Science Education (CIESESE) for giving us the opportunity to do this research.

References

[9] B.N.E Finance "Bloomberg". Retrieved on August 10, 2017 from: data.bloomberglp.com/bnef/sites/14/2017/01/BNEF-Clean-energy-investment-Q4-2016-factpack.pdf

[10] G.W.E. Council, "Global Wind Report 2016", GWEC. Retrieved on August 10, 2017 from: http://www.gwec.net/publications/global-wind-report-2/global-wind-report-2016/

[11] N. Geographic, "Wind Power". Retrieved on August 10, 2017 from: http://www.nationalgeographic.com/environment/global-warming/wind-power/

[12] IEEE, "ieeeexplore.iee.org". Retrieved on August 10, 2017 from: http://ieeexplore.ieee.org/document/7116959/

[13] D.Gitano-Briggs, "Small Wind Turbine Power Controllers", University of Science in Malaysia, Penang 6 Malaysia.

[14] Y. Yorozu, M. Hirano, K. Oka, and Y. Tagawa, "Electron spectroscopy studies on magneto-optical media and plastic substrate interface," IEEE Transl. J. Magn. Japan, vol. 2, pp. 740-741, August 1987 [Digests 9th Annual Conf. Magnetics Japan, p. 301, 1982]

Low energy consumption real-time tracker

Pedro De Jesús Morales[1], Fernando Arroyo Santos[2]
Department of Electrical & Computer Engineering, School of Engineering at Universidad del Turabo, Gurabo Puerto Rico
pde15@email.suagm.edu[1], farroyo19@email.suagm.edu[2]

***Abstract*—This project proposed a Mobile AdHoc Network (MANET) for real-time tracking of elements that do not provide an additional energy source. In wireless sensor networks, data transmission is the most energy consuming process. Therefore, it is important to reduce the amount of transmitted data in order to reduce energy consumption in mobile devices. In this project, the sensor and sink nodes are battery powered, and in order to provide portability, such battery cannot be heavily constraining the amount of power available. Therefore, the MANET must be optimized in order to provide real-time location of the tracked element as well as low-energy consumption. Low energy consumption materials such as the teensy microcontroller and radio frequency transceivers were carefully selected to maintain a low power consumption rate for this project. To properly display the power consumption, we first connected the teensy with the Xbee wireless transceiver in order to test and measure the consumed energy for transmitting data. The peak amount of current demanded using an Xbee is 68mA while transmitting. The second test consisted in connecting the teensy with the NRF24L01 wireless transceiver and, again, plot the current versus time graph to obtain the demanded current. After running the test twelve times for statistical significance, the peak demanded current was 42mA while transmitting. The results clearly show that the best wireless transceiver for low energy consumption is the NRF24L01 wireless transceiver.**

***Keywords*—transceiver; xbee; teensy; wireless; low power consumption**

I. Introduction

A wireless sensor network (WSN) is designed to gather data, perform an initial aggregation and transmit such data to a central infrastructure where the data is processed in order to produce useful information. The main characteristic of WSN is the portability and rapid deployment. A WSN define a set of sensor nodes and sink nodes. First, the sensor nodes sense and transmit the sensed data to the sink node. The sink node performs the first data aggregation and transmits the aggregated data to a central infrastructure. In wireless sensor networks, data transmission is the most energy consuming process. Therefore, it is important to reduce the amount of transmitted data in order to reduce energy consumption in mobile devices [1].

The sensor nodes are usually severely constrained in terms of battery, memory, CPU power, and communication capabilities. Battery-hungry mechanisms are usually not very appealing as the network availability will be affected [2]. On the other hand, a Mobile AdHoc Network (MANET) is a type of wireless network that does not require infrastructure for its operation. Therefore, every single node works as both a transmitter and a receiver. This particular feature makes it very appealing for rapid deployment in harsh and challenging environments. Thus, the most important applications of MANETS are in support of military special operations and civil emergency deployments, for instance, establishing communication networks and providing rescue services in natural disaster areas. In MANETs, nodes communicate with each other directly when both are within the same communication range; otherwise, the messages are relayed through their neighbors. MANETs, as any WSN, are energy-consumption constrained. During the design of a MANET, the energy consumption must be optimized in order to guarantee the availability of the network [3].

Since the data transmission is the most energy consuming process, the first step in this project is to select the correct data transmission protocol in order to guarantee low energy consumption as well as a relative wide coverage range. Therefore, this work presents the energy consumption results for the data transmission using an Xbee transmitter as well as the NRF20L01 transceiver.

The rest of the document presents the system design, experimental setup and result. Finally, the document presents the conclusion for this research.

II. System design

Figure 1 presents the proposed system architecture focusing on the data flow without the power lines. The sensor node is connected via wireless to the sink node.

The sensor node is a battery powered device which must sense the environmental conditions such as location using a GPS, position using a gyroscope and acceleration using an accelerometer. Notice that the sensor node in Figure 1 does not specify the actual sensors since this research focuses on energy consumption due to the transmission process between the sensor and the sink nodes. In addition, since sensor nodes do not require a high computational capability, the system architecture defines a microcontroller instead of a microprocessor in order to reduce cost as well.

On the other hand, the sink node includes a data receiver component as well as a processor since it requires a higher computational capability.

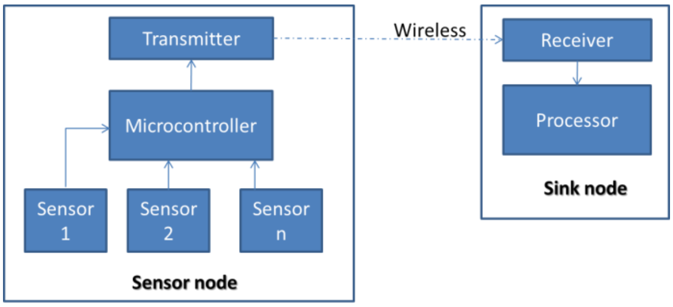

Figure 1. System architecture

III. Experimental Setup

The first step in this research consisted in finding a low-energy-consumption radio frequency (RF) transmitter. According to the literature, two RF technologies were suitable for this project. These two wireless options are the XBee and the NRF24L01. Additionally, in order to maintain low energy consumption, a teensy microcontroller was selected for the sensor node. This device uses a low voltage and consumes less current than most other microcontrollers in the market such as Arduino.

In order to graph properly the current consumption, an external power supply Keithley Series 2220 was used in order to power the sensor node. In this way, LABVIEW was used to read the actual current consumed by the sensor node as showed in Figure 2.

Figure 2. Reading setup

The Teensy 3.2 was the selected microcontroller since it has reduced energy consumption; in addition, this microcontroller is relatively small, which is a good option in order to guarantee the system portability.

A. Implementation using Xbee

The first Sensor Node implantation performed for this research was using the XBee 2mW Wire Antenna - Series 2 as showed in Figure 3. This module allows a reliable and simple communication between microcontrollers, computers, systems, really anything with a serial port. Moreover, the network configuration may be a point-to-point or a multi-point network according to the manufacturer [4]. In addition, the transmission range is up to 400 ft. according to the manufacturer.

The selected Xbee works with 3.3V and its frequency band is 2.4GHz. It is compatible with Teensy 3.2.

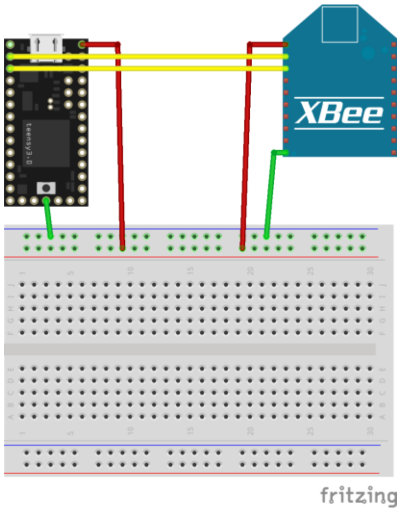

Figure 3. Sensor node implemented using a Xbee transmitter

B. Implementation using NRF24L01

The second implementation for the sensor node was using the NRF24L01 as showed in Figure 4. According to the manufacturer, this transceiver uses the 2.4 – 2.5GHz.

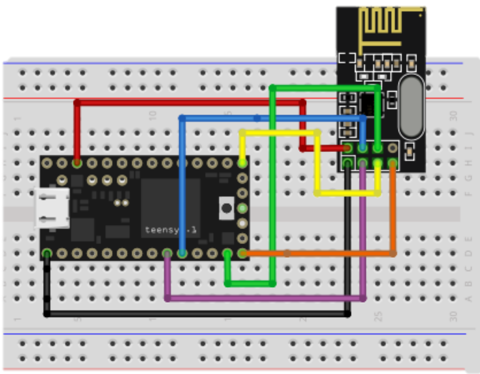

Figure 4. Sensor node implemented using a NRF24L01

Finally, Table I presents the bill of materials for this research. Notice that it includes additional parts for the integration of the transmitters and the microcontroller.

TABLE I. Bill of materials

ITEMS	COST
Teensy 3.2 with pins	$29.95 * 3 = $89.85
10PCS Arduino NRF24L01+ 2.4GHz Wireless RF Transceiver Module New	$6.29
XBee 2mW Wire Antenna - Series 2 (ZigBee Mesh)	$26.95 * 3 = $80.85
Gikfun Bluetooth XBee Shield V03 Module For Arduino EK1185_	$9.86 * 3 = $29.58
Teensy Arduino Shield Adapter	$12.95 * 3 = $38.85
Teensy 3.1 XBee Adapter	$12.95 * 3 =38.85

IV. RESULTS

This section presents the energy consumption results for each implementation.

A. Teensy 3.2 Microcontroller

Figure 5 shows the actual current that the Teensy consumes by itself. The power supply was setup to a voltage of 3.6VDC and a maximum current of 100mA to protect the circuit. As shown in Figure 5, the current remains constant in 38mA because the Teensy is not doing anything; it is idle.

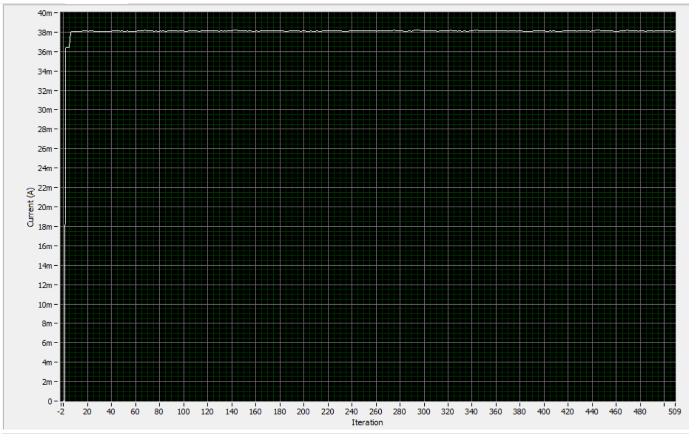

Figure 5. Teensy current consumption graph in LabView software

B. NRF24L01 Wireless RF Transceiver & Teensy

Figure 6 shows the current consumption of the NRF24L01 connected with the Teensy. This graph was obtained by using a power supply with a voltage of 3.6v, a max current of 100mA to protect the circuit and using LABVIEW to read the actual current consumed by the NRF24L01 connected with the Teensy. As shown in Figure 6, the current goes from 38mA to 41mA every time the NRF24L01 transmits data every second. Notice that the small peaks corresponds to the data transmission.

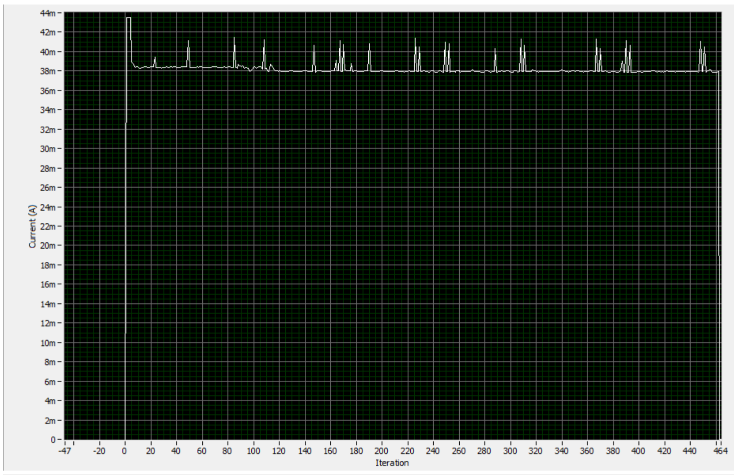

Figure 6. Teensy & NRF24L01 current consumption graph in LabView software while transmitting every second

C. XBee 2mW Wire Antenna and a Teensy 3.2.

Figure 7 shows the current consumption of the XBee connected with the Teensy. The power supply was setup to use a 3.6VDC, a max current of 100mA and using LABVIEW to read the actual current consumed by the XBee connected with the Teensy. As shown in Figure 7, the current goes from 48mA to 68mA every time the XBee transmits data every three seconds. The current starts from 48mA because XBee is with the Teensy; without the XBee transmitting, it consumes 48 mA.

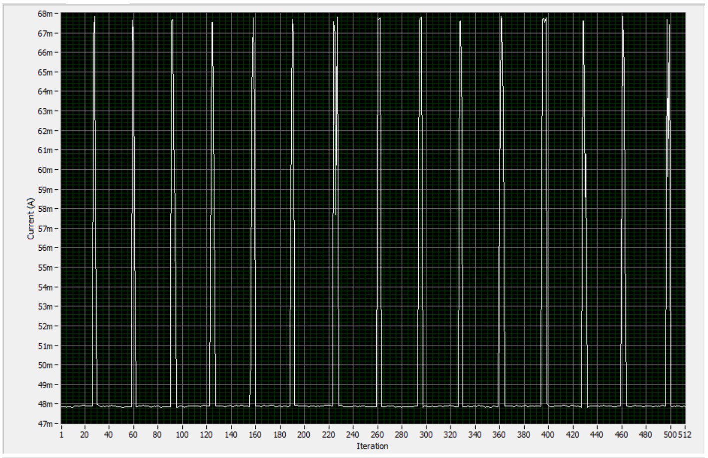

Figure 7. Teensy & XBee current consumption graph in LabView software while transmitting every three seconds

V. Conclusions

As shown in Figure 5 in this report, the Teensy consumed a constant 38 mA. The same test was performed with the NRF24L01 connected with the Teensy, and with the wireless module connected. Without transmitting, the system consumed only 38 mA. When the sensor node was transmitting using the NRF24L01, it consumed 41 mA as shown in Figure 6. When the XBee module was connected with the Teensy, without the XBee transmitting, it consumed 48 mA. When the XBee was transmitting, the current consumption raised to 68 mA, as shown in Figure 7.

After analyzing all these data carefully, without a doubt the wireless transmitter that consumes the less amount of power is the NRF24L01 wireless module. Testing will still be done to provide a better and more reliable data collection to properly show the exact power consumption of this wireless module. Working in the PREC Summer Research Camp was a very enriching experience and helped us understand better that research is the key to every discovery.

VI. References

[15] J. Stankovic, "Wireless sensor networks," *Computer*, vol. 41, no. 10, pp. 92–95, 2008.

[16] Q. Wang, M. Hempstead, and W. Yang, "A realistic power consumption model for wireless sensor network devices," in Proceedings of the 3rd Annual IEEE Communications Society Conference on Sensor and Ad Hoc Communications and Networks - SECON, Reston, Virginia, USA, September 2006, pp. 286–295.

[17] C. Bettstetter, G. Resta, and P. Santi, "The node distribution of the random waypoint mobility model for wireless ad hoc networks," *Mobile Computing*, IEEE Transactions, 2(3):257–269, 2003.

[18] XBee 2mW Wire Antenna – Series 2C (ZigBee Mesh). Available: https://www.amazon.com/XBee-2mW-Wire-Antenna-ZigBee/dp/B007R9U1QA/ref=sr_1_1?ie=UTF8&qid=1503553385&sr=8-1&keywords=XBee+2mW+Wire+Antenna+-+Series+2+%28ZigBee+Mesh%29

Optimal Wind Tunnel for Testing Small Scale Wind Turbines

Ian S. Maldonado[1], Jhonatan Carbajal[2],
Department of Mechanical Engineering, School of Engineering at Universidad Del Turabo,
Gurabo, Puerto Rico Department of Mechanical Engineering, Rensselaer Polytechnic Institute, Troy, New York
imaldonado45@email.suagm.edu[1], carbaj2@rpi.edu[2]

Abstract: **The goal set for this project is to be able to run tests on small-scale wind turbines using the present wind tunnel in Universidad del Turabo upholding the standards held by U.S. Department of Energy Collegiate Wind Competition. To achieve this a fan that is accommodated to the characteristics of the wind tunnel was chosen by the usage of fluid mechanics formulas and an Excel spreadsheet. Lastly a funnel and a pedestal were designed to accommodate the chosen fan in the current wind tunnel setup.**

I. Introduction

This project's objective is to be able to run tests on small-scale wind turbines using the present wind tunnel in Turabo university upholding the standards held by U.S. Department of Energy Collegiate Wind Competition.

Wind tunnels work with powerful fans that move air through a tube. The object to be tested is fastened in the tunnel so that it will not move and the object can be of small scale, full scale or even a piece of the object [1]. In the case of our project a small-scale wind turbine. The air moving around the still object shows what would happen if the object were moving through the air or how the air moves through the object [1].

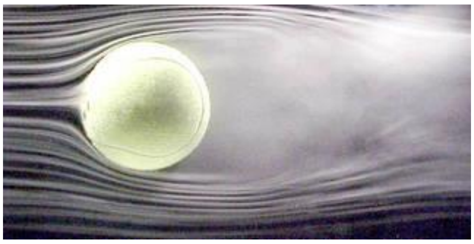

Figure 1: Wind flow on a tennis ball in a wind tunnel [1].

The U.S. Department of Energy Collegiate Wind Competition challenges undergraduate students to design a wind turbine based on market research, develop a business plan to market the product, build and test the turbine against set requirements, and demonstrate knowledge of opportunities related to wind farm siting. The objective of the Collegiate Wind Competition is to prepare students from multiple disciplines to enter the wind energy workforce [2].

For the wind tunnel to uphold the standards of said competition the tunnel should be able to run tests with continuous winds with speeds up to 20 meters per second [3]. To achieve this the correct fan to accommodate the characteristics of the current wind tunnel setup at Universidad del Turabo while being able to reach said speeds.

The fan selection process will be done by utilizing fluid mechanics formulas for volumetric flow and mass flow rates. The volumetric flow rate formula given by:

$$Q = VA$$

where V is the average fluid velocity and A is the cross-sectional area where the fluid is traveling, was used to determine the output velocity of the fan since the fans are often described by how much air volume they can move in CFM (cubic feet per minute) which is a volumetric flow rate unit. The mass flow rate formula given by:

$$\dot{m} = \rho AV$$

where ρ is the fluids density, A is the cross-sectional area where the fluid is traveling and, V is the average fluid velocity, was used in a relation between the cross-sectional area of the fan and the testing area to determine the velocity of the fluid in said area giving:

$$V_2 = \frac{A_1}{A_2} V_1$$

was used in a relation between the cross-section area of the fan and the testing area to determine the velocity of the fluid in the testing area.

II. Procedure

1. Study the specifications of the tunnel.
2. Identify the standards to achieve with said tunnel.
3. Search for equations that could enhance the process of meeting these standards given a certain fan.
4. Set these equations in an Excel spreadsheet, conversion of units included.
5. Test several options of fans that could meet the standards previously mentioned utilizing the Excel spreadsheet.
6. Pick the fan that best achieved the standards also being cost effective.
7. Design a funnel for the fan to best fit the current wind tunnel setup, and a pedestal to fit the current wind tunnel height.

III. Discussion and Results

To commence the investigation, it is necessary to first comprehend the competition's specifications for testing and the limitations of the wind tunnel present at Universidad Del Turabo. The measurements of the wind tunnel were used to narrow down the approximate testing area and to use in an equation that calculated the wind speed output from the selected fan. In using the CFM and radii of the Uline and Grainger fans, wind speeds ranging from $14m/s^2$ to $21m/s^2$ were determined. To accommodate the selected fan to the university's wind tunnel, special arrangements such as a funnel have been considered.

Figure 2: Wind Tunnel Setup at Universidad Del Turabo

Fans	Max theoretical speed on test section (m/s)	CFM low (ft^3/min)	CFM high (ft^3/min)
H-1575	18	15600	15600
H-1196	14	12500	12500
H-1576	16.8	14500	14500
H-1420	21	18200	18200
1YNW5	14	12250	12250
10R361	13.9-18.5	11971	14599
13F063	18.5	16000	16000
45LW12	14.5-19.7	12500	16800

Table 1: Speeds and Volumetric Flow Rates of each model considered.

As it can be seen on Table 1 a couple of the fan options provide with speeds at the testing area that are near the desired value at the time which was 18 m/s at the time the project took place. Since the standards have changed a testing area speed of 20 m/s has to be achieved some of the fans is no longer suitable for the task. For the new standards only the H-1420 from U-line and the 45LW12 from Grainger remain suitable for the task.

Fans	Cost excluding shipping ($)
H-1575	500
H-1196	389
H-1576	529
H-1420	579
1YNW5	573
10R361	514
13F063	755
45LW12	746

Table 2: Cost of each model.

From the two viable options, the most cost effective would be the H-1420 model from the U-line provider as it can be seen on Table 2. but sense this item does not ship to Puerto Rico the remaining option is the 45LW12 from Grainger.

IV. Conclusion

From the results of the calculations used to find the optimal fan for wind tunnel testing, the 45LW12 fan from Grainger was the most suitable one. Its high CFM of 16800 and fan diameter of 42 inches delivered a maximum calculated wind speed of 19.7 meters per second. On account of the wind tunnel testing area and collegiate wind competition regulations, the 45LW12 was chosen because it met the standards and it was the most economical choice considering that the H-1420 model can't be shipped.

V. References

[1] What Are Wind Tunnels? (Internet) Available from: https://www.nasa.gov/audience/forstudents/k-4/stories/nasa-knows/what-are-wind-tunnels-k4.html (Last accessed August 17, 2017)

[2]. About the Collegiate Wind Competition (Internet) Available from: https://energy.gov/eere/collegiatewindcompetition/about-collegiate-wind-competition (Last accessed August 17, 2017)

[3]. CWC Rules and Regulations (Internet) Available from: https://energy.gov/sites/prod/files/2017/07/f35/CWC%202018%20Rules%20and%20Regulations-web.pdf (Last accessed August 17, 2017)

VI. Apendix

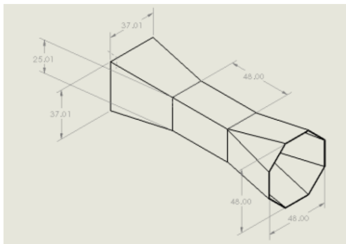

Figure 3: Isometric view of the wind tunnel at Universidad Del Turabo.

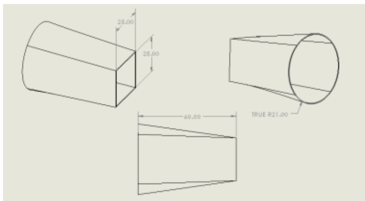

Figure 4: Drawing of funnel designed to fit current wind tunnel.

PV solar panel orientation for load following

Kenneth R. Mckenzie[1], Carl K. Camis Rosado[2], José Maeso[3]Department of Mechanical Engineering, School of Engineering at Universidad del Turabo, Gurabo, Puerto Rico, Electrical Engineering Caribbean University, Bayamon, PR
carlcamis@oumconn.com[1] kmckenzie1@email.suagm.edu[2], jgmaeso@prec.pr[3]

***Abstract*—We set out to confirm the applications of photovoltaic solar panel orientation from south-facing to west-facing configurations. Data is structured to compare the peak values of production for each of the two orientations mentioned, so we can compare and analyze the application of the west-facing configuration. Puerto Rico's electrical load peak do not match the peak generation of electricity from solar panels with an orientation to the south, making more difficult for the electrical system to integrate more renewable energy sources in an efficient manner. In simulation, moving the solar panels to a west-facing orientation has been found to shift the peak by two hours later into the afternoon, which presumably can contribute to the grid stability during peak load times. The data modeled using PVWatts Calculator helped us confirm that the production peak can be shifted to a later time in the afternoon, so that it could satisfy more efficiently the electric power load of Puerto Rico.**

***Keywords*—Solar, photovoltaics, peak load.**

I. Introduction

The focus of this project was to analyze how the energy production from a solar photovoltaic system compares between a south-facing and a west-facing array. The purpose was to evaluate if changing the most common setup for solar systems in Puerto Rico (south-facing) could help match the peak of the electric load of the Island. A software tool called *PVWatts Calculator* was used to simulate and analyze the two arrays.

The term photovoltaic (PV) means that solar cells convert light from the sun to usable electricity, using a structure similar to Figure 1. The system uses solar panels with semiconductor materials that display the photovoltaic effect. The direct current (DC) produced by the solar panels needs to be converted into alternating current (AC) format to be used in typical applications in homes and businesses.

To do this a power inverter is needed, which is a major component of a PV system. A typical PV system is shown in Figure 2. After the electricity is converted into AC, it is send to a power distribution unit that allows to divide the energy that is going to be used, for example, in a house, and any other remaining electricity is either stored or send to the electrical grid to be used someplace else [1].

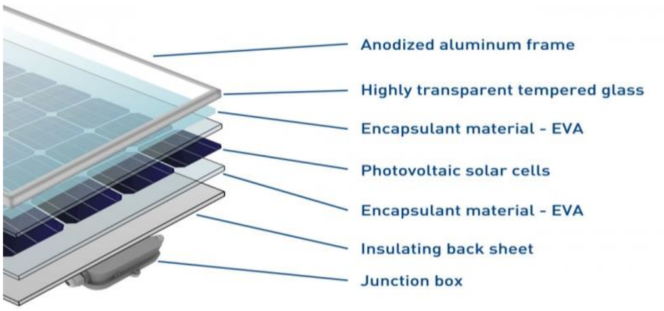

Fig. 1: Solar Panel Composition

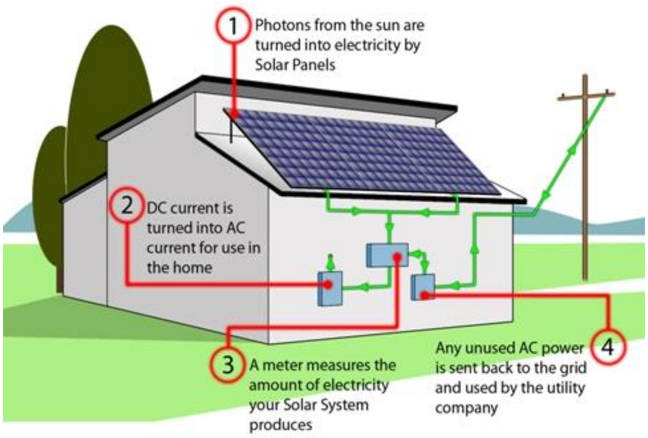

Fig. 2: PV System Diagram

In studies, it has been shown that the most optimum orientation for solar panels in the northern hemisphere is facing south. This is where they receive the most sunlight annually and produce the maximum amount of energy given by different parameters. When facing south, the PV system's working time intervals are between mid-morning and late afternoon hours. The problem with this time intervals is that the power that it is being produced does not match the grid load curve, making the grid more difficult to manage. This is because in many places, including Puerto Rico (P.R.), the peak grid load is precisely, during the late afternoon hours [2].

II. Methodology

In order to model the PV power production we followed the next steps:

1. We began by accessing pvwatts.nrel.gov website. The homepage provides standard information of

the National Renewable Energy Laboratory's (NREL) tool, as seen in Figure 3.

Figure 3: PVWatts Homepage

2. On the Get Started space we search for San Juan, Puerto Rico. The search will bring up the results of the Solar Resource Data for the region. It also provides relevant weather data of the location so it will match the environmental requirements.
3. After selecting the optional weather location, the right-hand side of the webpage provides the link for the section, *System Info* which we selected. We began with the south-facing configuration (Azimuth 180º; see Figure 4).
4. In the *System Info* page we entered 2 kW DC system size, 'Standard' module type, 'Fixed (open rack)' array type, 18º tilt, 180º array azimuth (for south orientation), we set the 14% standard system loss for all orientations, and a 96% inverter efficiency. DC to AC ratio remained at 1.1.
5. After all parameters are selected, we clicked on the 'Go to PVWatts Results' button. The page provided the results, which could be printed.

Location and Station Identification	
Requested Location	san juan, puerto rico
Weather Data Source	(TMY2) SAN JUAN, FL 5.4 mi
Latitude	18.43° N
Longitude	66° W
PV System Specifications *(Residential)*	
DC System Size	2 kW
Module Type	Standard
Array Type	Fixed (open rack)
Array Tilt	18°
Array Azimuth	180°
System Losses	14%
Inverter Efficiency	96%
DC to AC Size Ratio	1.1
Economics	
Average Cost of Electricity Purchased from Utility	No utility data available
Performance Metrics	
Capacity Factor	17.4%

Fig. 4: South-facing system parameters.

For the west-facing configuration system we followed steps 1 through 4. The key difference being that the 'Array Azimuth' was changed from 180º to 270º. All other parameters remained intact (see Figure 5).

Location and Station Identification	
Requested Location	san juan, puerto rico
Weather Data Source	(TMY2) SAN JUAN, FL 5.4 mi
Latitude	18.43° N
Longitude	66° W
PV System Specifications *(Residential)*	
DC System Size	2 kW
Module Type	Standard
Array Type	Fixed (open rack)
Array Tilt	18°
Array Azimuth	270°
System Losses	14%
Inverter Efficiency	96%
DC to AC Size Ratio	1.1
Economics	
Average Cost of Electricity Purchased from Utility	No utility data available
Performance Metrics	
Capacity Factor	16.3%

Fig. 5: West-facing system parameters.

For bigger systems, the 'Draw Your System' link lets you select the area to be used for the solar panel array. This is helpful for bigger configurations where the only data available is the footprint size.

III. Analysis and Results

A. South-Facing Orientation

The results given by the PVWatts platform for the south-facing configuration are shown in Figure 6. The total yield of the system is 3,055 kWh annually. The top four months of peak production are March, April, July, and August. 'Solar Irradiance' matches the production output variation, which is an indicator of the reliability of the platform. Current solar PV systems in Puerto Rico are generally installed using the south-facing configuration since it yields the most energy output throughout the year. For purposes of the simulation we will use two days, Monday 21 and Friday 25 of March 2016 (see Figures 7 and 9).

RESULTS

Print Results

3,056 kWh per Year *

System output may range from 2,972 to 3,137kWh per year near this location.
Click HERE for more information.

Month	Solar Radiation (kWh / m² / day)	AC Energy (kWh)	Energy Value ($)
January	5.15	244	N/A
February	5.57	238	N/A
March	6.08	286	N/A
April	5.98	273	N/A
May	5.52	259	N/A
June	5.64	257	N/A
July	5.76	269	N/A
August	5.79	269	N/A
September	5.85	263	N/A
October	5.40	253	N/A
November	4.84	220	N/A
December	4.76	224	N/A
Annual	5.53	3,055	0

Fig. 6: South-facing PV system results.

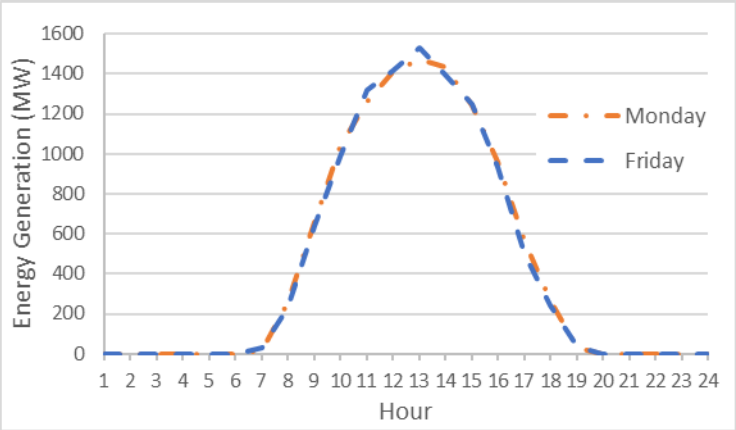

Fig. 7: South-facing PV system generation.

B. West-Facing Orientation

The data for the west-facing configuration showed a decline in total production of the system, which was expected. This data will help us determine the viability of matching the grid load peaks of Puerto Rico’s energy consumption with that of the solar PV peak energy output.

The total production output of the system with a west-facing orientation is 2,853 kWh per year, as shown in Figure 8. ‘Solar Irradiance’ captured by the system changes possibly due to orientation, which might have caused that the months of peak production change. The peak production of the modeled west-facing solar PV system were April, June, July, and August. With this information, in conjunction with the south-facing system data, we can compare the two orientations and see how well they match the grid load of the Puerto Rico Electric Power Authority (PREPA).

RESULTS

Print Results

2,853 kWh per Year *

Month	Solar Radiation (kWh / m² / day)	AC Energy (kWh)	Energy Value ($)
January	4.24	201	N/A
February	4.85	208	N/A
March	5.52	260	N/A
April	5.90	270	N/A
May	5.63	264	N/A
June	5.91	270	N/A
July	5.99	280	N/A
August	5.75	268	N/A
September	5.42	245	N/A
October	4.73	222	N/A
November	4.04	184	N/A
December	3.88	183	N/A
Annual	5.16	2,855	0

Figure 8: West PV System Results

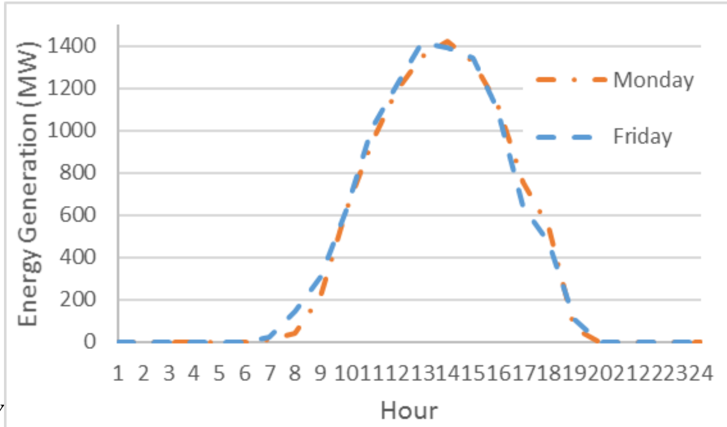

Figure 9: West-facing PV system generation.

Using data from PREPA for the month of March 2016 we compared the generation peaks between the two PV systems and the daily generation for that month—which matches the load in terms of variation. The peak daily generation is between 5:00 p.m. to 10:00 p.m. at any given day (see Figure 10) [3]. This is because during these hours people are getting home and start consuming a substantial amount of electricity when using appliances and lighting. This can result in a not reliable grid and causes problems if the load is too big and the production systems are not adjusted accordingly. Comparing the data between the two systems it can be shown that there is a small shift of one hour in the curve for the west-facing PV system production peak; in some cases it is only half hour (see Figures 11 and 12). This shift of the curve might not be enough to make a difference in the grid operation. For this to be a difference on the grid we will need a high-PV penetration scenario [2].

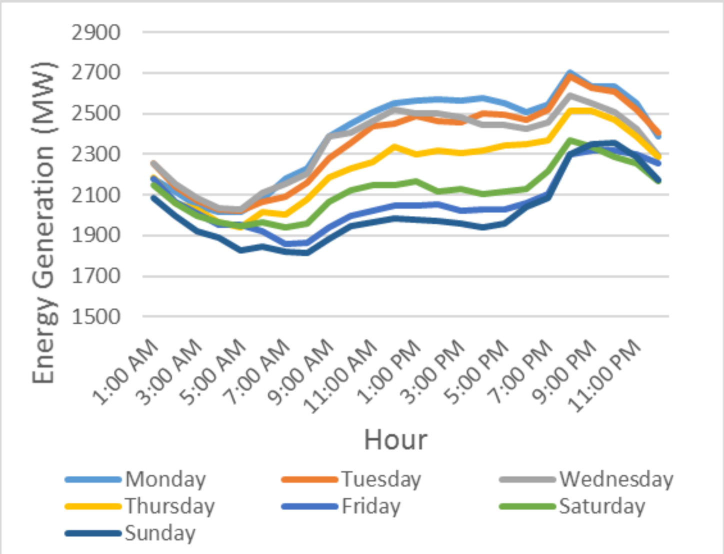

Figure 10: PREPA 'Daily Generation' (in megawatts) for one week of March 2016.

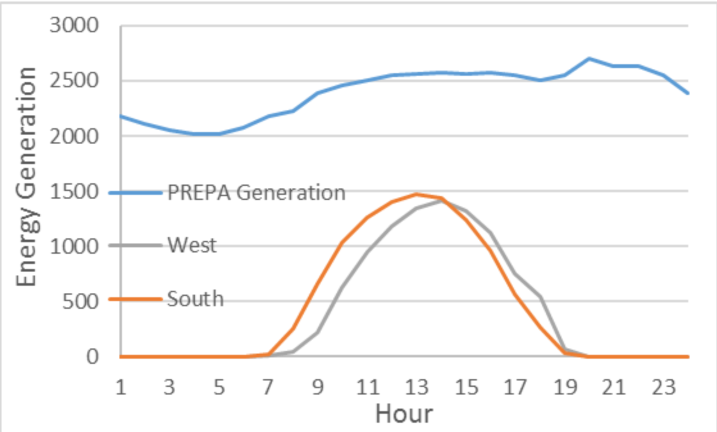

Figure 11: Comparison of south vs. west orientation on March 21, 2016.

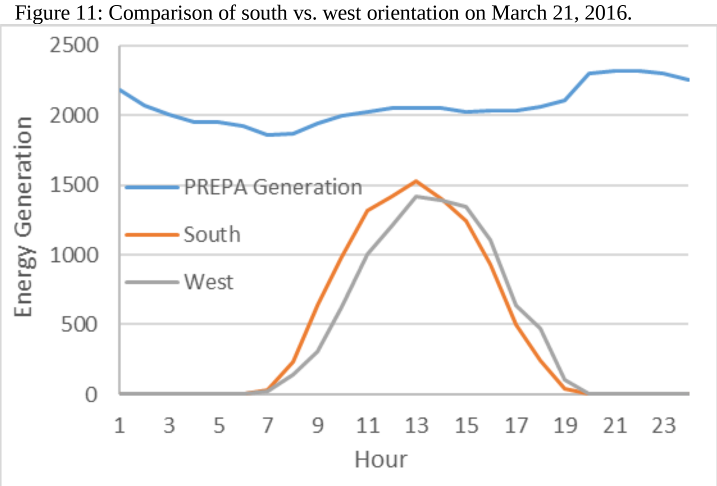

Figure 12: Comparison of south vs. west orientation on March 25, 2016.

IV. CONCLUSIONS AND FUTURE WORK

The laws and regulations in Puerto Rico are timid in the implementation of a high-penetration solar PV scenario, with a goal of only 15% of the energy production coming from renewable sources for 2020 (see Figure 13), as stated by PREPA.[5] This timing could allow PREPA to phase out fossil fuel production in small steps so a renewable energy substitution doesn't negatively impact grid stability. As we can see in the two systems comparison, the applicability for west-facing solar PV systems might not constitute a great impact to the electric load variations in Puerto Rico, until they constitute a significant portion of the generation.

The peak grid load of Puerto Rico starts late in the afternoon where no significant solar irradiance is available to replace fossil-fueled energy production. Nevertheless, west-facing systems at a large scale, could help ease the grid's stress by providing needed generation when the load starts increasing.

The next step for this research is to perform field measurements using the same parameters used in the

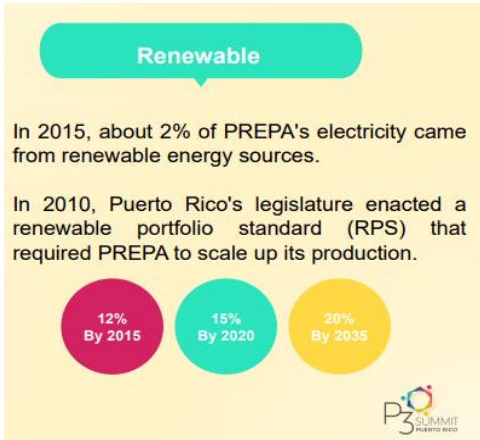

Figure 13: Puerto Rico's mandate for utility-scale renewable energy.

simulation of the PV systems to confirm there is a shift in solar PV peak production, accounting for weather variations and other variables.

V. REFERENCES

[1] T. Dahl, Photovoltaic Power Systems, 2015.

[2] A. Kankiewicz, West vs. south: Why change the orientation of your solar PV system, Clean Power Research, July 2015, originally published in the March/April issue of *Solar Today* magazine.

[3] Autoridad de Energía Eléctrica, "Informe de la Generación Diaria del Sistema Eléctrico," División Operación Sistema Eléctrico, Departamento de Operaciones, March 2016.

[4] Al Fin, "Intermittent Wind Cannot Replace Baseload Power," May 2012.

[5] Puerto Rico Public-Private Partnerships Authority, "Energy Projects," April 2017.

Waste materials from land fields and wetlands as energy source: Nitrogen profile of an urban wetland

Lewis Diaz-Torres[1], Ileana González-González[2], Department of Chemestry, School of Natural Science and Technology at Universidad del Turabo, Gurabo, Puerto Rico lewisdiaz1119@gmail.com[1], ilgonzalez@suagm.edu[2]

***Abstract*— The use of microbes for wastewater treatment has been reported in literature especially in microbial fuel cells (MFC) research. The advantages of using bacteria instead of the enzyme are robustness, cheapness and long-term use. A pilot assessment of microbial community and pH levels of both soil and surface water was performed last year but it was inconclusive. The scope of our project is to characterize the total nitrogen on the forest, including ammonia, nitrate and nitrite, which are essential to the growth of plants. The characterization of nitrogen overall will be performed in water samples. Other factors will also be measured such as temperature and pH. In our investigation, we determined the nitrite, nitrate and ammonia available. Measurements of pH and temperature were also recollected at the forest site. Preliminary samples collected during this summer we found low concentration of nitrate, ammonia and no presence of nitrite. Statistical analysis is needed to determine significant differences between parameters.**

Keywords—nitrogen; wetland; pterocarpus; microbial fuel cell

I. Introduction

The search for effective and less expensive energy is an idea of great interest in the scientific field, that is why it is sought to study the profile of nitrogen in the future also study the microbial community since the use of microbes for wastewater in cell research of microbial fuels has been reported in literatures. The proposal is based on investigating the nitrogen profile as mentioned in the pterocarpus forest of Palmas Del Mar in the town of Humacao. The genus Nitrosomes are the bacteria that are responsible for oxidizing NH_4^+ to NO_2 and they tolerate temperatures of 1 to 37° C, they have optimal growth at a pH close to neutrality (Pacheco J. et al, 2002). The nitrogen in the pterocarpus forest would be investigated further to be able to explain its profile and in the future of the research with better results a microbial cell. The process of nitrification and denitrification play an important role in the flora. Ammonification occurs before nitrification begins. Ammonification is the conversion of organic nitrogen found in wastewater in to ammonia/ammonium by the process of hydrolysis. The nitrification process begins when bacteria called Nitrosomonas biologically convert ammonia/ammonium into nitrite. The conversion of nitrite to nitrate is then carried out by the bacteria Nitrobacter. Levels of nitrite are usually low but have been increasing overtime, causing a major impact to the greenhouse effect. These processes predominantly occur in aerobic conditions, hence free dissolved oxygen is necessary. Temperature and pH are factors that affect the process of nitrification. Denitrification is the biological reduction of nitrate to nitrogen gas by facultative heterotrophic bacteria. Facultative bacteria need carbon (organic material) to perform the denitrification process. This process occurs under anoxic conditions, there for levels of dissolved oxygen are very low. Due to poor solubility of nitrogen gas in H_2O the nitrogen is released in the air causing no concern to the environment. This process is carried out under alkaline conditions. The growth rate of denitrifying organism is limited by temperature. Annamox organisms are a group of bacteria that oxidize ammonium using nitrite instead of oxygen to produce nitrogen gas instead of nitrate. This process is performed under anaerobic conditions called anaerobic ammonium oxidation or annamox. This process is considered uncommon and occurs at a slower rate in comparison with conventional nitrification and denitrification process.

II. Methodology

Several water samples were taken in the marshy *pterocarpus* forest at Palmas del Mar in Humacao. The first sample taken was to examine the presence of nitrite in water. The water was deposited in a 10mL vial, the Hanna Instruments reagent (HI 3873-0) was used to determine the presence of nitrite, then measured on a colorimetric scale ranging from 0.2mg / L to 1.0mg / L. In the second sample, the presence of nitrate was determined, another Hanna Instrument reagent (HI 3874-0) was used for the presence of nitrate, then the water was deposited in the vial showing the colorimetric scale ranging from 10mg / L up to 50mg / L to determine the presence of nitrate. The third sample was to determine the presence of ammonium. An ammonium-specific Hanna Instrument kit was used; The water was deposited in the 10mL vial, the vial was placed in the low range ammonium colorimeter HI700 which should be in C.1, then waited until C.2 appeared, the vial was removed and 4 drops were added Reagent A, stir gently, then add 4 more drops of reagent B, after 3.30 minutes the results are obtained in units of ppm ammonia nitrogen (NH 3 -N). Finally, samples of salinity and pH were performed, for the salinity test a pHep Tester of Hanna Instrument was used. For pH, a Hanna Instrument

Waterproof Tester was used for pH and temperature measurement.

III. Results

In the preliminary tests in the forest, the samples were taken in shaded areas and where the sun gave directly, were significant. On the first day of the sample, the first location being a shaded area, there was ammonia (NH3), which resulted in 0.93ppm (ammonia); In the second location that was in an area where it gave the sun, the result was 0.16ppm (ammonia). There was also nitrate (NO3) although at a low concentration of 10mg / L in both locations, the shade and where the sun. When the sample of nitrite (NO2) was realized there was no such, but we believe that if nitrite is present below the measurement standards. The factors for microbiological oxidation are because it occurs rapidly under aerated conditions with temperatures between 15 to 30 ° C and a pH of 6.5 to 7.5 (Pacheco J. et al, 2002). The genus Nitrosomes are the bacteria that are responsible for oxidizing NH_4^+ to NO_2 and they tolerate temperatures of 1 to 37° C, they have optimal growth at a pH close to neutrality (Pacheco J. et al, 2002). In the pH samples, the temperature (° C) was also measured. In the first location, the pH was 7.13 ± 0.01, a temperature of 29.1° C and in the second location the pH was 7.62 ± 0.01, a temperature of 29.3° C. A salinity sample was attempted but it could not be performed because the instrument used was not functioning well and the result obtained could not be relied upon.

On the second day of sampling, the tests were performed under the same conditions except that the water level to be sampled in the forest was higher than the first day and the locations were relatively distant from the first. The order in which the samples were taken was the same, the first location was where the sun was directly, there was ammonia (NH3), the result was 1.3 ppm ammonia and in the shaded location was 1.9 ppm ammonia. When the nitrate sample (NO3) was performed there was no such or it is believed that it is below the measurement parameters in both locations; As well as when the nitrite (NO2) test was performed it could also not be detected or it will be in a low concentration in which it cannot be within the parameters to measure it. As for the samples of pH and temperature taken, there was a significant change, in the first location the pH was of 7.25 ± 0.01, temperature of 32.2° C, in the second location the pH was of 6.93 ± 0.01, temperature of 30.1° C.

IV. Conclusion

In conclusion, based on the preliminary analyses, it was perceived that obtaining samples in shaded areas and in areas where the sun is directly influencing the expected result. Also, it was observed that the level of water in the forest has an effect, since in the ammonia sample there was an increase in the ppm of the results because in the first day there was not so much water level, but the second day there was a high-water level, It can be said that there was also a lot of organic material from which the sample was taken, since one of the characteristics of the forest is the high amount of organic matter in the soil and water. The nitrogen profile will continue to be investigated in order to have a clearer explanation of these results, so far, the information obtained is superficial and therefore the reason or the effects of the results obtained cannot be determined. For future plans, with more information collected we can have a clearer view on the profile of nitrogen in the Forest *pterocarpus* in Palmas Del Mar (Humacao) and thus make the relevant tests to be able to add a microbial cell as the main objective of this work in base to energy.

Acknowledgment

The author would like to acknowledge the Puerto Rico Energy Center (PREC), Dr. Ileana Gonzalez and graduate student Yariann Cardona for the opportunity given during this research. We are also grateful to Wesly Martínez, a guide to the Pterocarpus Forest and to Palmas del Mar, for allowing investigations to be carried out and opening the door to new prospects.

References

[19] Adams, D., Hefner, J. and Dopazo, T. (1999). Puerto Rico, humedales [Puerto Rico, wetlands]. *U.S. Geological Survey*, pp.1-6.

[20] Pacheco Ávila, J., Pat Canul, R. and Cabrera Sansores, A. (2002). Análisis del ciclo del nitrógeno en el medio ambiente con relación al agua subterránea y su efecto en los seres vivos. *Ingenieria*, 6(3), pp.73-81.

[21] Rivera, Wilmer O., (2011). *Eficiencia en el uso de los nutrientes: nitrógeno (N), fósforo (P), y potasio (K) en especies arbóreas utilizadas en las áreas mitigadas de la ciénaga las cucharillas* (tesis de maestría). Universidad Metropolitana, Puerto Rico.

[22] Weaver, Peter L. 1997. *Pterocarpus officinalis* Jacq. Bloodwood. SO-ITF-SM-87. New Orleans, LA: U.S. Department of Agriculture, Forest Service, Southern Forest Experiment Station. 7 p.

Vertical Axis Wind Turbine Generator

Oscar A. Faura Molina1, Xavier G. López Correa2, Department of Electrical and Computer Engineering
At the Universidad del Turabo Gurabo, Puerto Rico, ofaura@email.suagm.edu1, xlopez13@suagm.edu2

***Abstract*— This paper reports on a modelling of a coreless permanent magnet synchronous generator (PMSG) with an axial magnetic flux to be used on a vertical axis wind turbine. The design incorporates the working principle of an electric generator which contain a stator and a rotor. The stator or field winding is composed of nine magnetic copper wire coils and the rotor or armature winding is composed of twenty-four rare earth magnets, better known as neodymium magnets. Core is not used in the stator of the machine intended to be designed. Aim of this research is to provide both reduction of iron loss and making the machine become lighter. Moreover, easiness in the production stage of the machine is provided. Within this research, arrangements have been made depending on certain standards in order that permanent magnets and coils produce three-phase alternating current. The designed axial flux generator will have a maximum voltage of approximately twelve volts per phase.**

Keywords: PMSG, VAWT, stator, rotor, neodymium magnets, AFPM

List of symbols

B_{mg}	Magnetic flux density on magnet surface (T)
B_r	Remanent magnetic flux density (T)
$f_{nominal}$	Generator nominal frequency (Hz)
E_f	Electro-magnetic force (V)
g	Mechanical clearance gap (mm)
H_c	Coercive field strength (A/m)
h_m	Permanent magnet thickness (m)
h_r	Back-iron thickness (m)
k_{sat}	Saturation factor
l_a	Active length (m)
$n_{nominal}$	Nominal RPM
p	Number of pole pairs
q	Total number of coils per phase
Q	Total number of coils
t_w	Stator axial thickness (m)
w_m	Permanent magnet radial width (m)
μ_0	Vacuum permeability (Wb/(A·m))
μ_{rrec}	Recoil permeability

V. Introduction

Axial-flux permanent-magnet (AFPM) machines have many unique features. For being permanent magnet, they usually are more efficient, as field excitation losses are eliminated, reducing rotor losses significantly. Machine efficiency is thus greatly improved, and higher power density achieved. Axial-flux construction has less core material, hence, high torque-to-weight ratio. Also, AFPM machines have thin magnets, thus are smaller than radial-flux counterparts. AFPM machine size and shape are important features in applications where space is limited, so compatibility is crucial. The noise and vibration they produce are less than those of conventional machines. Their air gaps are planar and easily adjustable.

In small scale applications, the usage of small wind turbines to generate energy is a usual practice, when connection to the grid is not a possibility or when high price rates exist. Small wind turbines have a varied range of nominal power values and often use permanent magnets to create the generator's excitation field. The usage of permanent magnets in a coreless axial flux generator makes the manufacture process easier and appropriate for the development of the hardware for the application. Using these designs, with some equations, the generator can be designed and manufactured according to the nominal power needed. In this report, an explanation of these basic theoretical concepts and manufacturing method is presented.

In the preliminary steps of the design process, the type of connection to be utilized must be contemplated. The generator output will be rectified through a full wave bridge rectifier (Figure 1). When the turbine's rotor blades start gyrating, the generator output voltage $V_{cut\text{-}in}$ must be equal to the load voltage. This occurs when the wind increases to the cut-in wind speed v_w. This wind speed is often set at 3 m/s for small applications.

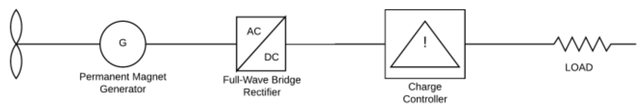

Figure 1: Block Diagram of the generator

VI. Wind Turbine

Assuming a cut-in voltage of $V_{cut\text{-}in}=12\ VDC$ and given that the wind turbine will start operating at wind speed of $v_w=3\ ^{m}/_{s}$, other generator characteristics can be calculated. In this case, the tip speed ratio is not constant, but decreases as the wind speed increases, due to lower voltages in the stator that limit the rotational speed of the generator's rotor and thus slow down the rotor blades. To achieve the optimum value of the tip speed ratio λ at a typical average wind speed of about 4-5 m/s, the tip speed ratio is set at 8.75 for the cut-in wind speed. Assuming a $\eta = 90\%$ generator efficiency during nominal conditions and given the nominal output power $P_{nominal}=60W$, the turbine radius $R_{turbine}$ can be calculated by (1). Setting the aerodynamic power coefficient at $C_p=0.35$ for the optimal tip speed ratio at nominal wind speed, where the aerodynamic power is (2), where η is the generator efficiency, where the air density at sea level is $\rho = 1.2\,\frac{kg}{m^3}$.

$$R_{turbine}=\sqrt{\frac{2P_{air}}{\pi\rho C_p v_w{}^3}} \tag{1}$$

$$P_{air}=\frac{P_{nominal}}{\eta} \tag{2}$$

VII. Choosing the Generator Frequency, Pole Pairs and Coil Number per Phase

Since the generator output voltage will be rectified, choosing a specific nominal frequency will be more relevant to the total cost of the generator than its operational characteristics. This is because the nominal frequency $f_{nominal}$ (i.e. the frequency at nominal wind speed) determine the number of poles pairs p given by equation (3) and thus the total number of magnets. In this case, the frequency of the generated voltage does not limit the design since the operation of the generator, which consists of a first stage of rectification and then another one of inversion, allows the generation to be at a frequency other than 60 Hz. However, it will be considered that the higher the frequency generated, the more the insulation of the current will be facilitated and the ripple of the voltage at the output of the rectifier will be reduced.

Therefore, in order not to obtain a too low frequency or a machine too large, it is decided that the wind turbine consists of 12 poles. Given the chosen configuration, front rotor and rear, both with magnets, will be necessary 24 magnets for the development of the machine.

The permanent magnets used in this design are circular neodymium magnets (NdFeB) which are the most expensive and rare material used in the generator. Nevertheless, according to the literature [1], there are cases when the reduction of the number of poles pairs result in reduced efficiency and distorted voltage waveforms and harmonics.

$$p=\frac{120f_{nominal}}{n_{nominal}} \tag{3}$$

The number of optimum coils to be used is directly related to the number of poles by (4) The coils are connected in a three-phase system using a wye-connection, each phase consists of three coils.

$$n_{coils} = \frac{3}{4}\cdot p \tag{4}$$

The proper pole pair to coil combination for creating a three-phase system are presented in Table 1.

TABLE II. Poles- Coils Combination

Poles-Coils Combination	
Poles	***Coils***
8	6
12	9
16	12
20	15
24	18

VIII. The Generator Axial Dimensions

The axial dimensions of the generator (Figure 3) include the thickness of the back-iron rotor disk, the thickness of the magnets h_m, the mechanical clearance gap g and the thickness of the stator t_w. Having chosen the most cost effective commercial magnets to be found that are suitable for the application and are used in, their thickness and grade are set and are $h_m=3.175\ mm$ and the grade are N52, while the diameter is 25.4 mm. The mechanical clearance gap g is chosen at 3 mm and consist of 1 mm of mechanical gap, 1mm of resin over the magnets and 1mm of resin over the stator coils. A reduction on the total air gap could be achieved by minimizing the thickness of the resin layer over the magnets and the stator, resulting in higher induced voltage and higher power output. The resin layer over the neodymium magnets should not be eliminated though, because is protect them from corrosion. Also, the gradual degradation of the bearing need to be considered resulting in possible future misalignments of the bearing shaft that might cause friction between the stator and the rotor and would produce a more robust generator. An increase in the mechanical clearance gap without a reduction in produced power could be achieved with the use of stronger magnets.

The axial thickness of the stator coils can be calculated by (5), which result from the analysis of the magnetic circuit while assuming zero magnetic flux density leakage. The magnetic flux density near the magnet's surface B_{mg} is usually set at about $\frac{B_r}{2}$, where the remanent magnetic flux density B_r and the coercive field strength H_c are characteristic values of the magnet that are related to its grade and can be easily extracted from the neodymium magnet data sheet. Other variables are $k_{sat} = 1$ due to the coreless stator and μ_0 the vacuum permeability.

$$B_{mg} = \frac{B_r}{1+\mu_{rrec}\frac{(g+0.5t_w)}{h_m}k_{sat}} \tag{5}$$

$$\mu_{rrec} = \frac{B_r}{\mu_0 H_c} \tag{6}$$

If NdFeB N52 magnets are chosen, then equation (5) can be rewritten for the thickness of the stator as:

$$t_w + 2g = 2h_m \rightarrow t_w = 2h_m - 2g \tag{7}$$

The thickness of the back-iron disk is complex to calculate from theoretical equations. Some general characteristics of the back-iron disk can be stated though. The back-iron disk thickness should be reduced as much as possible to avoid increases in total weight of the generator, but as the same time it should not be reduced too much to withstand the attractive magnetic forces pulling the two rotor disks together and thus ruining the mechanical clearance gap and damaging the generator. Also, magnetic saturation is possible in the iron disk if it is chosen too thin. A practical "rule of thumb" states that the back-iron thickness should be equal to the magnet's thickness. The attractive forces between the rotor disk are the main factor that influence the back-iron thickness.

The average radius of the machine is related to the power delivered by the wind turbine using the following equation (8):

$$P_{nominal} = \pi BKR_m{}^2 l_a n_{nominal} \cos\varphi \tag{8}$$

From equation (8) we can obtain the average radius that the projected machine must have, considering that the rest of variables are known or can be estimated. The power generated $P_{nominal}$ must be at least 60 W. The remaining magnetic induction B_r is a little more complex to define since its value strongly depends on the distance between the magnets of the front and rear rotor. Initial calculations were made with B_r=1.48T. The specific linear load K cannot be set with complete accuracy. However, after studying various references in the literature that mention this factor, it was decided to fix it at $K = 150\ \frac{A}{cm}$. Since circular magnets are to be used, the length of the active area l_a is conditioned by these as can be seen in figure 2. That is, l_a is equal to the diameter of the magnets: l_a=25.4mm. The mechanical angular speed of the machine is determined by design criteria. It is desired that the wind turbine can operate at low wind speeds, which allows the support tower not to be too high. For this reason, $n_{nominla} = 300$ rpm. The power factor is set at $\cos\varphi = 0.8$ which is the most usual value.

Using the equation (3) to determine the nominal output frequency, we can state that $f_{nominal}$=30Hz.

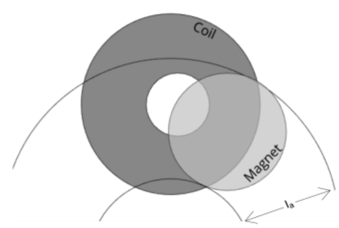

Figure 2: Active Length of the generator

IX. The Generator Winding Dimensions

A coil has four main characteristics that define it: the induced voltage at its terminals, its external and internal diameter and the number of turns it should have. In this case, the phase voltage is known as a design criterion. It is desired to obtain a phase voltage equal to 12 V. Considering that the phase voltage is equal to the terminal voltage of each coil multiplied by the number of coils in each phase (as already mentioned above is three coils per phase). Therefore, the terminal voltage of each coil E_{coil} must be 4 V.

The electromotive force induced in each coil is calculated from the flux density of the first harmonic. If the inductive coupling of a coil is (9):

$$\lambda = \hat{\lambda}\omega t \tag{9}$$

where λ is the inductive coupling, ω is the angular speed and t is time. Then the induced EMF is obtained through Faraday's law as (10):

$$\mathrm{E_{coil}} = \frac{2\pi}{\sqrt{2}} f \hat{\lambda} = 4.44 f \hat{\lambda} \tag{10}$$

where $\mathrm{E_{coil}}$ is the induced EMF, f is the electrical frequency and $\hat{\lambda}$ is the inductive coupling.

However, the inductive coupling cannot be calculated directly since the flux density is distributed sinusoidal. Therefore, to do the calculations, it will be assumed that the coil is concentrated in its axial mean position, but that the coil is divided into several segments in its radial direction with the turns of each segment concentrated in the middle radius of each segment.

Using basic equations for electromagnetic induction and assuming an almost sinusoidal magnetic flux density $\mathrm{B_{mg}}$, the required turns per coil can be calculated in a simplified way. Initially, the maximum flux per pole Φ_{max} is calculated using (11):

$$\Phi_{max} = \mathrm{B_{mg}} \cdot \mathrm{w_m} \cdot \mathrm{l_a} \tag{11}$$

where $\mathrm{w_m}$ is the magnet's width and l_a is the magnet's length and the active length of the generator (Figure 2). Then the number of turns per coil $\mathrm{N_c}$ are calculated using (12), where $\mathrm{k_w}$ is a winding coefficient equal to 0.95, q is the number of coils perphase, n is the RPM at cut-in and $\mathrm{E_f}$ is the corresponding induced EMF voltage during cut-in:

$$\mathrm{N_c} = \frac{\sqrt{2} E_f}{q \cdot 2\pi \cdot k_w \cdot \Phi_{max} \cdot n \cdot {}^{p}/_{120}} \tag{12}$$

X. The Manufacturing Process

All the issues analyzed previously are mainly concerned with the design process of the generator, while emphasis is given at specific points that need to be considered to complete the construction phase without any major problem.

The construction of the generator begins with constructing the coil winding tool (Figure 3). This simple tool is made from aluminum frame and a straight rod and consist of two parts. Two outer disk with an inner spacer (Figure5).

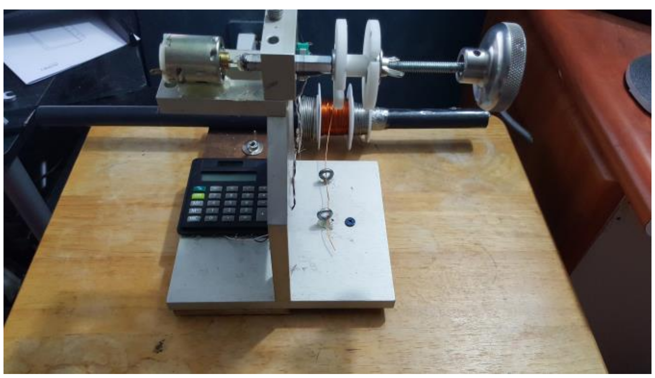

Figure 3: Coil winding tool

The spacer sets the axial thickness $\mathrm{t_w}$ of the coils and thus of the stator. For winding the coils, it is essential to carefully count the turns, to make sure one turn of copper conductor is set next to the other and to tense the conductor enough, as this results in less gap in between the turns of copper conductors and thus more successful coils.

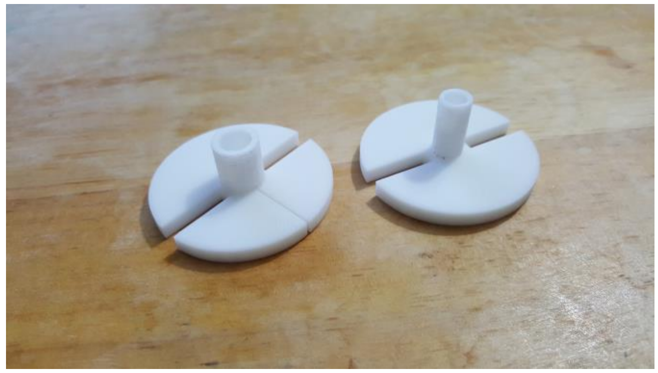

Figure 4: Coil disk

Figure 5: Assembled coil disk

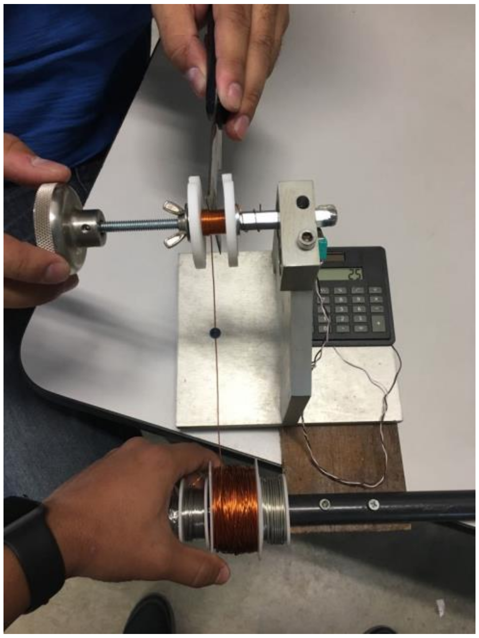

Figure 6: Winding the coils

Almost all the parts are designed in solid works with the exact measurement for the better fitment of the parts. The diameter of the generator is 8.25 inches. The size was designed with the measurement of the neodymium magnets of one inch diameter and the measurement of the coils that consist with a center space of half inch and the thickness of the coil is half inch the total size of the coil is one-and-a-half-inch diameter (Figure 7). The two parts of the rotor was fabricated in a 3D printer with ABS plastic filament. It took around 24 hours for each part for print.

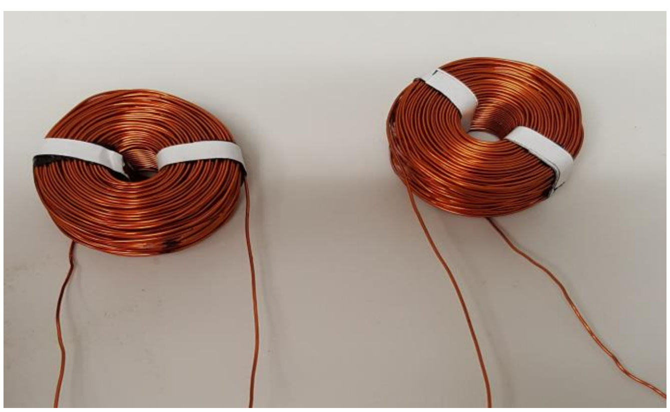

Figure 7: Coils

Figure 3: All coils, shape of the stators

The Rotor is designed that the neodymium magnets is totally incrusted in the rotor. In the center of the rotor it has a bearing so is more easily to spin (Figure 7).

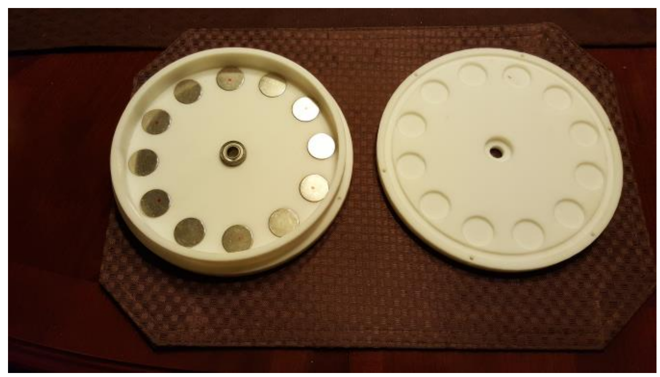

Figure 8: Rotor top and bottom

To compensate the weight problem the rotor was made not complete filled but was reinforced in the inside (Figure- 9). Has almost the same strength as if were a solid piece.

Figure 9: Inside part of the rotor

The assembled rotor will fit exact with the stator with an airgap of 1mm. as shown in the figure 10 has the design of the final product, the rotor and stator.

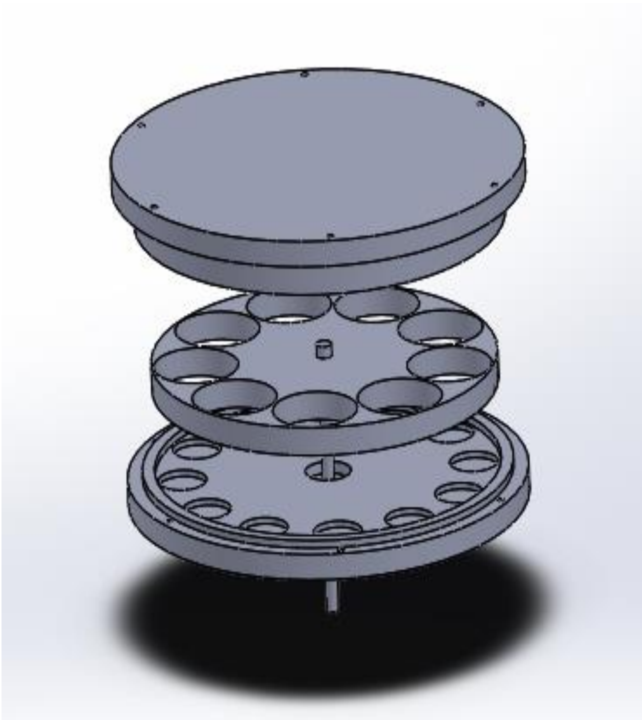

Figure 10: Final assembly solidworks

XI. Conclusion

In this paper, we demonstrate the principles of a permanent magnets vertical generator that will be producing 12v to supply a street light bulb. The generator will consist of a two-piece rotor, will be holding 24 neodymium magnets 12 magnets the top part and 12 magnets the bottom part. The stator will have 9 coils 3 for each phase for a total of 3 phase system. The coil winding machine was fully made to make with less difficult the coils. Each coil has 400 turns of a 22awg magnet wire. The system is designed to start producing at a minimum speed of 5 miles per hour.

XII. References

1. Bumby, J.R.: “Axial-flux, permanent magnet electrical machine”, British Patent Application No 0412085.3, 29th May 2004
2. H. Piggott, A Wind Turbine Recipe Book-The Axial Flux Windmill Plans, 2009.
3. J.F. Gieras, RJ. Wang and MJ. Kamper, Axial Flux Permanent Magnet Brushless Machines, 2nd ed. Springer, 2008.
4.

Use of Vegetation for Energy Efficiency Improvement

Abel J. Concepción Negrón[1], Luz E. Torres Molina, PhD[2], Department of Civil Engineering, School of Engineerng at Universidad del Turabo Gurabo, Puerto Rico,
aconcepcion30@email.suagm.edu, torresl6@suagm.edu

Abstract*— Energy saving and efficiency are some of the main topics used in the modern world to promote the increase of sustainability and reduce pollution produced by the generation of fossil fueled powered electricity. The main goal of this study is to assess indoor air quality and determine energy efficiency, in a study room, using plants. The plant used for the research was the Spathiphyllum, best known as peace lily. Air conditioning systems have a purpose of ventilation or air refreshment, and temperature control. The function of ventilation is to reduce CO_2 concentrations in enclosed spaces. CO_2 is a known indoor pollutant affecting performance in the workplace, at school, and offices around the world. Extreme levels of CO_2 may be harmful to health and safety of individuals. Levels of CO_2 in the range of 800 ppm and 2,500 ppm in the office and classroom have been found to decrease concentration and performance, and rates of absenteeism. Indoor plants play an important role in lowering indoor CO_2 levels, hence reducing the energy requirements of the buildings. For this research, plants were added to the room EDI 146 at the engineering building with the aim of lowering the CO_2 levels produced by students' breaths and low ventilation. One plant was added for every hundred square feet with a total of seven plants. CO_2 levels were measured in the room throughout seven months, other factors were considered such as number of people in the room, air temperature, wet bulb temperature, dew point temperature and relative humidity. A decrease in CO_2 levels will reveal if the energy efficiency was improved by the implementation of indoor plants. A statistical analysis was performed to explore the relationship between different variables.

***Keywords*— Spathiphyllum, Carbon Dioxide, Temperature, Relative Humidity, Energy, Indoor Air Quality**

I. INTRODUCTION

In the seventies, when the energy crisis began, buildings had been constructed significantly lowering the exchange of indoor and outdoor air. The main aim has been to save energy costs by re-circulating internal air and minimizing the need to heat, cool or condition outdoor air. Although considerable savings are achieved with this strategy, unwanted pollutants can and do become trapped in these tight enclosures. A pollutant such as CO_2 may have negative effects on human health that are caused by poor indoor air quality.

The indoor CO_2 level is one commonly used approach which has been referred as an indoor air quality indicator [1]. When CO_2 level reaches 800-2500 ppm, humans begin to feel tired and sleepy. According to the American Society of Heating Refrigerating and Air Conditioning Engineering, higher CO_2 concentrations can cause headaches, nausea, faintness or even fatality. It is known that people react differently to varying levels of distinct substances. These potentially adverse effects are further complicated by the fact that people are spending more time than ever indoors, up to 90 percent per estimates by the U.S. Environmental Protection Agency (EPA). It is easy to understand why there is a growing concern about the quality of the air that people breathes and its relationship with the energy saving.

There is doubt about the amount of fresh air needed to maintain a balance between health and energy savings. When too little outside air inside a room there are negative health affects previous mentioned. On the other hand, when too much outside air inside a room there are excess energy cost and a possible HVAC (Heating, ventilation and air conditioning) overload.
People are always looking for a way to improve the air quality in their homes, apartments and offices. Therefore, Indoor plants could play an important role in lowering indoor pollutants levels, specifically CO_2.

By purifying air, plants remove chemicals in the air as well also absorb carbon dioxide through their stomata, and then release oxygen [2]. Another way they help cool the house is by adding humidity to the room, plant release moisture into the air through the process of transpiration.

II. OBJECTIVE

The engineering building at Universidad del Turabo has several study rooms that are available for students twenty-four hours through the seven days of the week. One of the concerns about these study rooms without doubt is the environment quality and students comfort.

The main aim was to assess indoor quality, examine the influence of occupant density on the indoor air parameter in the study room EDI 146 at Universidad del Turabo and determination of energy efficiency using plants in this study room. The indoor air quality was tested ensuring that levels of CO_2, temperature, and relative humidity are kept inside the ASHRAE standard recommendations.

The plants used for this research were Peace lilies. They are one of the most common plants to be found on houses. According to the University of Minnesota while all plants absorb carbon dioxide and release oxygen as part of the photosynthesis process, peace lilies also absorb airborne pollutants such as benzene, formaldehyde and trichloroethylene [3].

III. MATERIALS AND METHODS

An indoor air quality research requires several steps. The first step was determining the research area. This was selected according to the greater number of people concentrated into the rooms. Another reason to select this room was that it be open to students as long as possible and easily accessible.

Determine the strategy to be employed. The AQM4 CO_2 meter by CO2Meter Inc. was selected as the equipment to be used for the indoor quality test and data gathering. The meter starts measurements when powered on and updates readings every second. The meter possesses a measuring range from 0 to 9999 ppm for CO_2, a range of -20 to 60℃ for temperature and a range of 0.1 to 99.9% for relative humidity. The uncertainty is $\pm$30 ppm, $\pm$ 0.6℃, and $\pm$3% respectively.

The samples were conducted between two and four in the afternoon (2:00pm and 4:00pm), with ten (10) minutes ranges. An average of six samples per day was gathered. The number of occupants, which varied throughout the day, was recorded in each sample; furthermore, temperature, relative humidity and other products were recorded. As far as possible the measurements were conducted every day and continued for four working days during the week by a period of six months. After these six month seven plants were added to the study room with the purpose to observe and measure the temperature, CO_2 and relative humidity. The Associated Landscape Contractors of America suggest one plant per hundred (100) square feet (9.29 square meters). The room where the research is conducted has an area of seven hundred and twenty (720) square feet (30’x24’); therefore, seven plants were added. [4]

Other important product measure in this research was the relative humidity. The relative humidity is directly related to human comfort. Too little humidity in a space may create static build-up and people will sense that their skin feels dry. Too much humidity and people will think it feels “sticky.” According to ASHRAE Standard 55, indoor humidity levels should be maintained between thirty (30) percent and sixty five (65) percent for optimum comfort [5]. Lower levels in humidity can cause eye irritation; higher levels can induce microbial growth in the area [6]. ASHRAE further recommends that concentrations of carbon dioxide (CO_2) be maintained below eight hundred (800) ppm in offices or indoor areas with presence of people and the ASHRAE recommends temperatures between twenty and twenty four (20 and 24) ℃.

The airflow is an important measure factor when talking about indoor air quality. Unfortunately, this product could not be measured for lack of funds. However, the ASHRAE requires that classrooms be provided with 15 cfm/person for outside airflow to the classroom [7].

Plants as a natural mechanism of pollutant catcher and air purification were used. The photosynthetic process that allows plant to live and grow requires a continuous exchange of gaseous substances between plant leaves and the surrounding atmosphere. The most common gaseous substances exchanges are carbon dioxide, oxygen and water vapor. The plant leaves normally give off water vapors and oxygen and take in carbon dioxide.

However, it appears that plants leaves can also take in other gaseous substances from the surrounding atmosphere through the stomata on their leaves.

IV. ANALYSIS OF RESULTS

The data collection began from January 2017 without use of plants. Since month of June the Spathiphyllum plants were placed at the study room EDI 146. The environment characteristics inside and outside the room and students attendance are continuously varying through the academic year into the room. The occupant's number was changed constantly.

Throughout the research, it was possible to gather data at the study room with 1 student inside the room until 30 students, see Figure-1 (appendix I). It is appreciable that once the plants were added the CO_2 levels started to drop; there wasn't much change between five and eight people, however, as the number of occupants increased the drop in CO_2 levels became noticeable.

In much of the collected data, lower CO_2 levels were registered with the implementation of Spathiphyllum plants in the room. Along with the highest number of occupants the maximum CO_2 value present without plants was found to be nine hundred and fifty four (954) ppm. As of first instance the levels of CO_2 seemed to increase as the number of people increased, therefore, a dispersion graph was created.

By developing the dispersion graph, a correlation was found between the two variables, number of occupants and the CO_2 levels, proving that the CO_2 levels did increase with the number of occupants, see Figure-2 (Appendix II).

A consistent relationship between the occupancy and corresponding carbon dioxide concentrations was seen in the study.

In fourteen instances, CO_2 levels exceeded 800 ppm. A calculated Pearson correlation coefficient of 0.9343 was found, which means that a strong positive linear correlation was obtained. The determination coefficient was found to be 0.8731, which represents that 87.31% of the variation in the CO_2 levels is explained by the variation in the number of occupants into the study room.

Table-1 shows an environmental variables distribution of data recorded in the room during the summer months. An equal number of trial days with and without plants were chosen. A median, minimum, maximum and standard deviation analysis was executed, with a range of 5 to 12 people. This range was selected for the plants were added in summer, when the student's attendance is lower.

TABLE III. AVERAGE ENVIRONMENTAL VARIABLES DISTRIBUTION USING SUMMER DATA.

	CO_2 No Plants (ppm)	**CO_2 With Plants (ppm)**	**Temp. No Plants (℃)**	**Temp. With Plants (℃)**	**Rel. H No Plants (%)**	**Rel. H With Plants (%)**
Median	817.75	683.67	20.72	21.17	68.65	68.18
Min.	746.33	534	19.80	20.74	66.80	64.57
Max.	920.25	703.5	22.88	22	73.65	71.4
SD	66.31	57.99	0.96	0.46	2.62	2.07

Although all data were analyzed; to do the comparative analysis it was necessary to work only with the summer data. Seven weeks between May and June months were selected; some weeks using the plants and other without plants. This methodology was done to avoid the greatest number of factors that can produce uncertainty.

The data collected and analyzed were CO_2, Temperature and relative humidity. For this comparison analysis was taken an average of 8 occupants because this was the occupant's number more recurrent during this period. The data were taken between 14:00 and 16:00 local time.

As show in Figure-3 the CO_2 values using plants decreased considerably. Measured levels showed a decrease near to three hundred (300) ppm once the plants were added.

This ample difference between the CO_2 levels is due to an extreme event recorded, however, the average difference in the CO_2 levels with and without plants is closer to the 100 ppm. A critical day was considered to show the potential difference in CO_2 levels that can be achieved.

Figure-4 led to discover a 2℃ drop once the plants were added. The graph showed a constant behavior through time, the 2℃ decrease can be appreciated at any given point. Between Figure-4 and Figure-5 it is appreciable that temperature and relative humidity are inversely proportional, as temperature rises, the relative humidity decreases. Human comfort must be taken into consideration in the decision of increasing the temperature for energy saving.

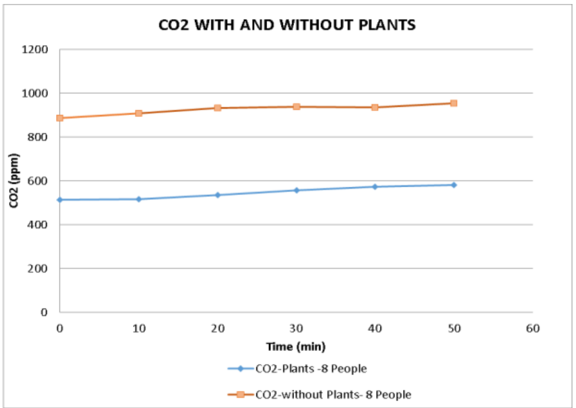

Fig. 1. CO_2 levels comparison with and without plants for 8 occupants during summer period, selecting only one day with and without Spathiphyllum, where greater difference was found.

Unlike the other graphs, Figure-5 didn't show a big difference in the relative humidity percentage. It shows a similar behavior with or without plants; however, it increased a bit more with the Spathiphyllum plants added.

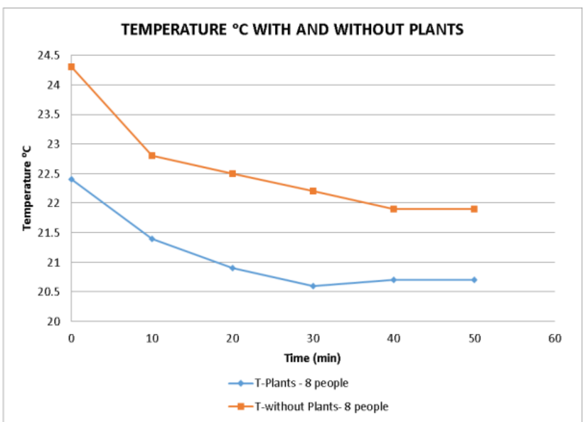

Fig. 4. CO_2 levels comparison with and without plants for 8 occupants during summer.

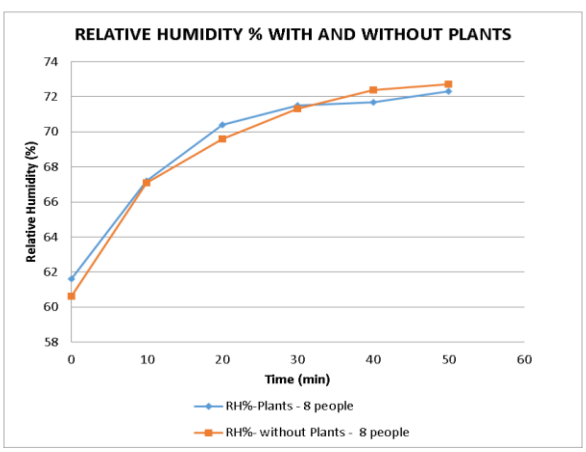

Fig. 5. Relative humidity comparison with and without plants for 8 occupants selecting only one day with and without Spathiphyllum, where greater difference was found.

Figure-6 presents the carbon dioxide levels outside the studied room. Levels recorded were much lower, at no moment it comes close to 500 ppm, therefore, the CO_2 levels inside and outside the room showed a significant difference.

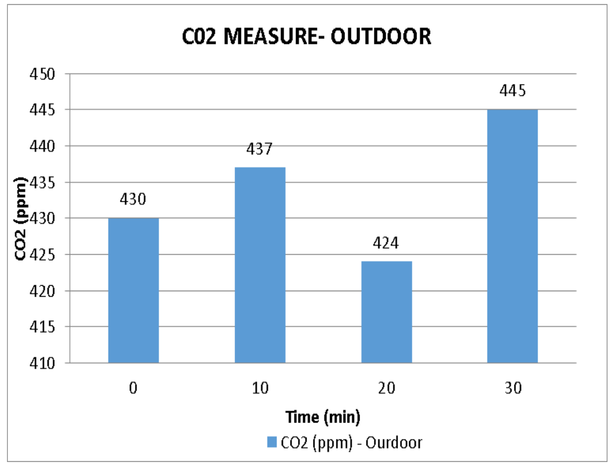

Fig. 6. CO2 levels outside the building.

V. Conclusion

With data around the 1000 ppm the performance of individuals in schools and offices with elevated CO2 concentrations can be affected because occupants may become lethargic and drowsy. [8]

Additionally, as CO_2 builds up, so do other indoor air contaminants, which increases occupants' exposures to irritating, distracting and potentially unhealthy gases and particulates.

This study revealed that CO_2 levels are directly affected by the amount of people present in the room. The highest CO_2 level during summer was found to be nine hundred and twenty (920) ppm with twelve people; almost five hundred (500) ppm greater than CO_2 levels registered outside the room. This value is alarming since it almost equals the maximum value recorded throughout the study with less than half of the occupants.

Taking this into consideration, installing carbon dioxide monitors in all classrooms would be suggested. CO_2 levels were close to 1000 ppm in different occasions with a maximum occupancy of thirty students. As mentioned before, high CO_2 levels could have a negative effect on students' performance. Around thirty students participate in each lecture; the performance of students is very important, so it is necessary to maintain an environment with low levels of CO_2 at all times.

Furthermore, an airflow meter can be implemented in the classroom to verify that the air conditioner equipment is working correctly and meets the established requirements by the ASHRAE 62. An average of around a hundred (100) ppm was achieved by the implementation of the seven Spathiphyllum plants. No relationship was found between carbon dioxide levels and temperature; however, the data revealed that temperature and relative humidity are inversely proportional.

In Figure-4 a drop of 2℃ was discovered, this drop in temperature could lead to energy saving for the desired temperature set in the thermostat of the air conditioner equipment can be reached faster. The thermostat will verify the room temperature, if the desired room temperature was reached the compressor will stop working, which leads to energy saving. A one degree difference means that eight percent less of the energy is being consumed by the equipment. [9] The drop in temperature was found with seven plants, the number of plants do play an important role in the outcome. This drop was registered in an extreme event; however, this shows the potential that plants possess. The experiment could be developed differently, only one plant could be added to see the effect it has on the room, and progressively add more plants as weeks go by. As it is known, all plants have different characteristics and behave differently in distinct environments. The study could be replicated with a different species of plant; therefore, different results will be achieved.

ACKNOWLEDGMENT

My acknowledgement with high appreciation goes to "Fondo Especial de Fomento de Investigación de la Oficina del Presidente de la Universidad del Turabo" for the equipment used in this research.

REFERENCES

[23] Lin, Z. & Deng, S. (2003), The outdoor air ventilation rate in high-rise residences employing room air conditioners. Build. Environ., 38, 1389-1399.

[24] Element Mountain, Plant Respiration- Revised, Publication date: Nov. 2014 URL:http://elementmountain.com/den-post/plant-respiration-revised/

[25] L. Deitz, What Are the Benefits of Peace Lilies?, URL:http://www.gardenguides.com/124066-benefits-peace-lilies.html

[26] [4] R. Pavlis, A garden myth is born, Publication date: Dec. 2014 URL: http://www.gardenmyths.com/garden-myth-born-plants-dont-purify-air/

[27] TSI Incorporated, Indoor Air Quality handbook, Publication date: 2013

[28] North Carolina Energy Office, Ventilation and indoor air quality, Publication date: Apr. 2010 URL:https://ncdenr.s3.amazonaws.com/s3fs-public/Environmental%20Assistance%20and%20Customer%20Service/IAS%20Energy%20Efficiency/Opportunities/Ventilation_and_Indoor_Air_Quality.pdf

[29] Trane, Designing an ASHRAE 62-compliant ventilation system, Vol.24 Publication date: 1995

URL:https://www.trane.com/content/dam/Trane/Commercial/global/products-systems/education-training/engineers-newsletters/airside-design/enews24_2.pdf

[30] Washington State University, Measuring Carbon Dioxide Inside Buildings – Why is it Important? Publication date: Jan. 2013

URL:http://www.energy.wsu.edu/Portals/0/Documents/Measuring_CO2_Inside_Buildings-Jan2013.pdf

[31] Agencia de gestión de energía de la región de Murcia, La energía que gastamos en nuestros hogares

URL:http://www.agenergia.org/files/resourcesmodule/@random493ea37fa7d61/1228844162_Fichas_sobre_ahorro_energetico_ARGEM.pdf

[32] K. Ponsoni, Gonçalves Raddi, M., Indoor air quality related to occupancy at an airconditioned public building, Publication date: Jan. 2010.

APPENDIX I

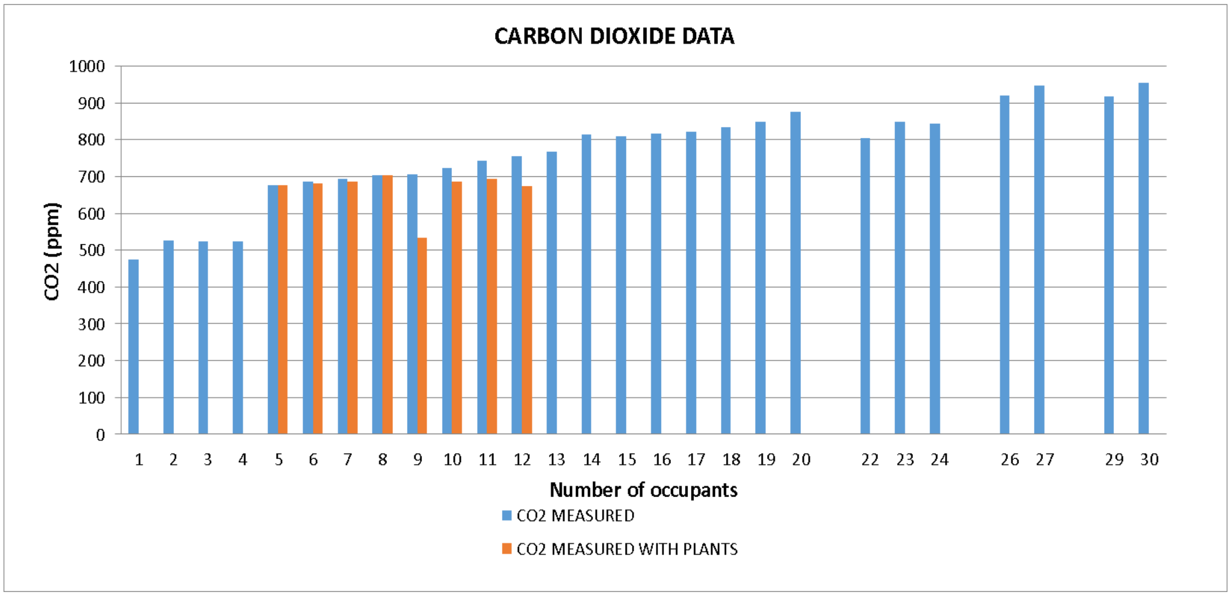

Fig. 1. Carbon dioxide levels average with and without spathiphyllum in different number of occupants.

APPENDIX II

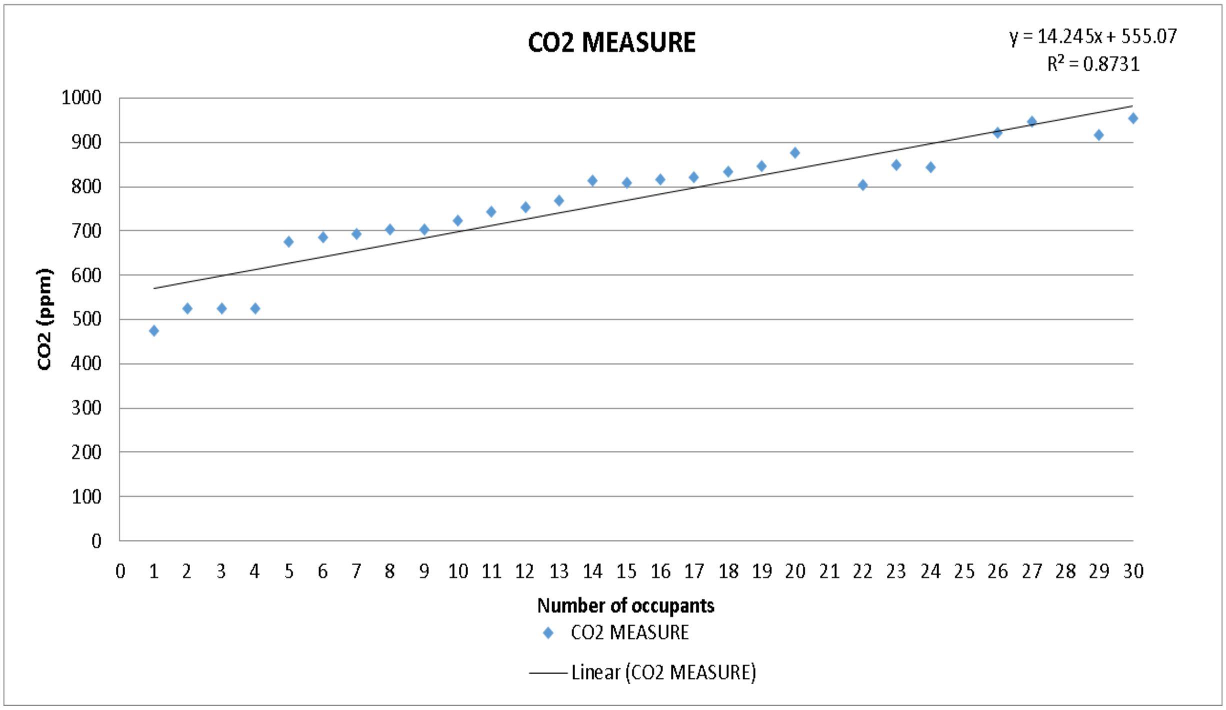

Fig. 2. Occupation and indoor Carbon dioxide level inside the air-conditioned room without Spathiphyllum.

Bacterial Bioprospecting for Bioenergy Applications: Xylose Fermentation

Edwin G. Velázquez-Pérez*, Jonathan López-Carrasquillo*, Janmary Colón Alicea, Claribel Báez, José R. Pérez-Jiménez Puerto Rico Institute for Microbial Ecology Research, School of Natural Sciences and Technology, Universidad del Turabo, Gurabo PR 00778
*equal contribution to the research

Abstract— **High dependency to fuel based on carbon fossil has been a major problem during the 21st century. Researchers have been looking for more economic and eco-friendly sources to bring energy to the world. It has been proposed that the xylose fermentation of plant residues is a suitable source of biofuels. Our goal is to characterize xylose-fermenting bacteria (XFB) and resulting alcohol production. Preliminary xylose fermentation was demonstrated by growth on media containing xylose as sole carbon source. Putative XFB were initially described by microscopic examination of Gram stains, catalase, and response to Chromagar® Orientation. Total genomic DNA was extracted for the amplification and sequencing of their 16S rDNA gene. Alcohol production was determined by Ritter test (qualitative) and nuclear magnetic resonance (NMR; quantitative). Thirteen XFB strains were obtained, nine (9) acidified the media showing potential alcohol production. Seven of them were selected for further testing because reacted faster than others. Two of those cultures were centrifuged and the supernatant was distilled to obtain the alcohol. Once the possible alcohol was obtained, it was analyzed by nuclear magnetic resonance. Analyses are in progress for definitive results.**

Keywords—Xylose, Alcoholic Fermentation and NMR

I. Introduction

At present, there is a great demand for fossil fuels, which are very limited and are known to contribute to climate damage. This has led to the search for new alternatives to produce clean, economic and sustainable energy (1, 2, 3). This is where biofuels arise as non-fossil sources of energy. Biofuels are all those derived from the biomass of recently living organisms or their metabolic products such as biodiesel and bioethanol (4). Forest, agro-industrial and agricultural wastes are considered as renewable, economical and abundant energy sources. Those accumulates every year, but are usually ignore for further use (3).

Bioethanol are less polluting than other fuels and of great utility in the energy area. Ethanol is produced through the fermentation of sugars derived mainly from agricultural products such as sugarcane, corn, sorghum or cereals (3, 4, 5, 6). Fermentable sugars in plants are usually embedded in lignocellulosic-based fibers that limit their bioavailability. Lignocellulose consists mainly of cellulose, hemicellulose and lignin, closely related polymers found in the plant cell. Hemicellulose, abundant in wood, is a heterogeneous linear and branched polymer normally composed of more than five sugars (L-arabinose, D-galactose, D-glucose, D-mannose, and D-xylose) and other compounds (i.e., acetic, glucuronic, and ferulic acids). These can be found as a homopolymer or heteropolymer by classifying it as constituted (7). Hemicellulose remains as an amorphous compound allowing a greater hydrolysis than cellulose, and release of D-xylose for further ethanolic fermentation (3). This process can be carried out by bacteria, yeasts and fungi through enzymes called xylanolitic enzymes (8).

The study of xylanolitic enzymes is very common in filamentous fungi, but very few of these are known in bacteria. Bacterial β-xylosidases and endo-xylanases on *Bacillus*, *Cellulomonas*, *Micrococcus* and *Staphylococcus* strains have been characterized (8). The discovery of more bacterial strains capable of fermenting D-xylose and producing viable ethanol for mass use suggest biocatalysts more efficient for particular process conditions. Bacteria grow faster and less expensive than fungi alternatives. The slow fungal growth make industrial processe less cost-efficient.

Therefore, our main objective is to identify bacterial strains are capable of fermenting D-xylose into ethanol.

II. Methods

General Microbiology and Molecular Procedures. A bacterial collection was activated and propagated as pure culture on Tryptic Soy Agar. Gram stain demonstrated morphological traits. Metabolic capabilities tested catalase production and response to Chromagar® orientation. Xylose fermentation was demonstrated on media containing phenol red pH indicator. Positive fermentation turned the red media to yellow; showing a more acidic environment. Total genomic DNA was extracted from each putative XFB for the amplification and sequencing of their 16S rDNA gene.

Nuclear Magnetic Resonance analysis. A more specific approach to identify the molecule of ethanol was performed using Nuclear Magnetic Resonance (NMR) with an

Ascend Aeon 400. For this, 45 mL of inoculated media was centrifuged for 10 min. at maximum speed. The supernatant was conserved for extraction. Simple distillation was used to obtain potential ethanol present on the supernatant. The phase was collected from 78-84 °C. A small portion from the extraction was used separately for Ritter test and NMR analyses. Samples used in NMR were dissolved with chloroform-D.

Ritter test. Once the bacteria fermented xylose and the possible alcohol was distilled, the Ritter test was performed to determine the presence of primary and secondary alcohols. This test used 1 mL of acetic acid and 1 drop of potassium permanganate per 300μL of sample. In presence of primary and secondary alcohols, the test will turn from pink to a light brown.

III. Results and discussion

Strains. Using general media, we obtain a total of 13 different strains. Twelve of them was Gram positive and one was Gram negative. From those strains, four of them was coccus and nine were bacillus (Table 1). All the thirteen strains proved to be positive to catalase test showing the capability of breaking the hydrogen peroxide by using the catalase enzyme.

TABLE 1. Preliminar Microbial Characterization

Strain	Gram Reaction	Shape
W1	positive	cocci
W2	positive	bacilli
W3	positive	bacilli
W4	negative	coccus
W5	positive	coccus
W6	positive	bacilli
W7	positive	bacilli
W8	positive	bacilli
W9	positive	bacilli
W10	positive	bacilli
W11	positive	bacilli
W12	positive	bacilli
W13	positive	coccus

Fermentation. Bacterial fermentation of xylose was proven by inoculating strains on xylose containing media. Four turned the media more alkaline and nine turned the media more acidic (Table 2); showing possible production of alcohol. However, the fastest strains in growth and turning the media acidic were selected for further analysis.

TABLE 2. Xylose Fermentation

Strain	Reaction in Fermentation Media
W1	acidic
W2	acidic
W3	acidic
W4	acidic
W5	acidic
W6	acidic
W7	acidic
W8	alkaline
W9	alkaline
W10	alkaline
W11	acidic
W12	alkaline
W13	acidic

CHROMagar™ Orientation reaction. Strains with positive fermentation were inoculated on CHROMagar™ Orientation media. This media provides the most diverse distinctive pattern within the media collection for presumptive identificaction. XFB strains developed metallic blue colonies (Figure 1) corresponding to the *Klebsiella, Enterobacter* or *Citrobacter* strains group. However, it contradicted Gram stain descrition and 16S rDNA sequencing results. The XFB includes members of *Bacillus* and *Enterobacter*.

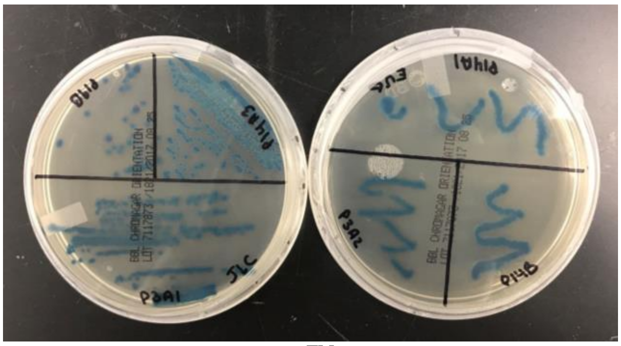

Figure 1. Chromagar™ Orientation results

Nuclear Magnetic Resonance. Two samples were selected for NMR analyses because they performed the fermentation faster. Those two strains were centrifuged at maximum speed for 10 min and simple distillation was done resulting on clear fractions (Figure 2).

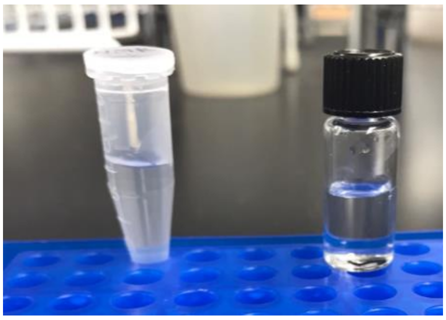

Figure 2. Obtained solution from the simple distillation

The signals obtained in an NMR spectrum are due to the forces of an external magnetic field applied to the protons found in a specific molecule. This field affects the position of the spins acting as a micro-magnet which interacts with the magnetic field of the external magnet by emitting a signal that is detected by a probe found near the sample inside the NMR equipment. These signals are unique depending on the chemical equivalence of each molecule. In our case, it was expected to obtain three signals from our sample (Figures 3 and 4). Also, in each signal can be found peaks (multiplicity) that give us an idea of how many protons are interacting with neighboring nuclei in the molecule possessing magnetic moment. Chemical shift is another value that can be seen in the NMR spectrum, each proton has a specific value depending on its position (bond) in the molecule. These signals, peaks and values shown tell us which molecule is the one found in our sample. According to the observed, we found that the sample obtained and studied is ethanol, this test does not give a quantification of the sample, only gives a characterization of it.

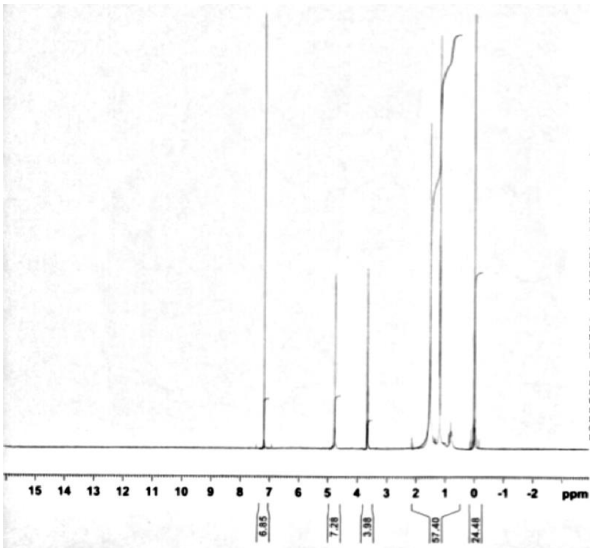

Figure 3. NMR profile for strain W2

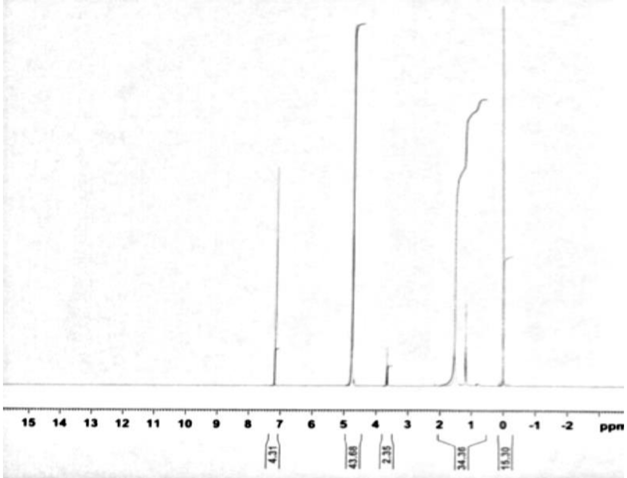

Figure 4. NMR profile for strain W2

Ritter Test. This test was performed to get another confirmation of possible alcohol presence on the distilled solution. Positive result was shown for the samples as they change the initial solution from pink to an uncolored solution (Figure 6). It was expected to turn the pink into a browner color as the test indicate, however turning the solution clear indicate that further studies must be done to confirm the presence of alcohol.

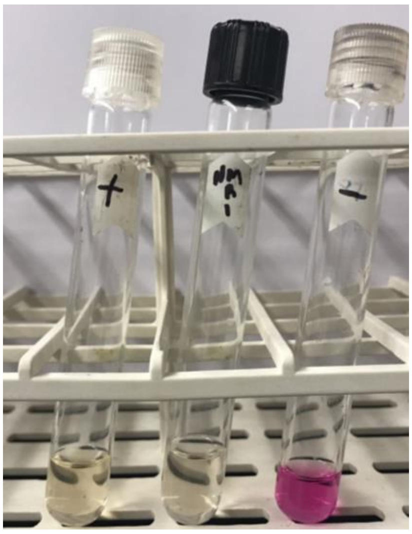

Figure 6. Positive control, Sample and Negative control for the Ritter Test

In conclusion, ethanol production from bacterial xylose fermentation was demonstrated from strains morphologically different. The potential for bioethanol production from plant residues, as xylose, suggest alternative catalysts towards efficient bioprocesses deserving additional research.

References

[1] Y. Kim, L.O. Ingram, K.T. Shanmugam. “Construction of an *Escherichia coli* K-12 Mutant for Homoethanologenic Fermentation of Glucose or Xilose without Foreign Genes.” Applied and Environmental Microbiology, vol. 73, no. 6, pp. 1766-1771, 2007.

[2] C. Bi, J.D. Rice, J.F. Preston. “Complete Fermentation of Xylose and Methylglucuronoxylose Derived from Methylglucuronoxylan by *Enterobacter asburiae* Strain JDR-1.” Applied and Environmental Microbiology, vol. 75, no. 2, pp. 395-404, 2009.

[3] S.I. Mussatto, A. Teixeira. “Lignocellulose as raw material in fermentation processes.” Portugal: IBB; 2010.

[4] A. Friedmann, R. Penner. “Biocombustibles Alternativa de negocio. [Biofuels Alternative business.]” Paraguay: Alejandro Sciscioli, de la Unidad de Comunicaciones del programa Paraguay Vende; 2009.

[5] K. Ohta, D.S. Beall, J.P. Mejia, K.T. Shanmugam, L.O. Ingram. “Metabolic Engineering of *Klebsiella oxytoca* M5A1 for Ethanol Production from Xylose and Glucose.” Applied and Environmental Microbiology, vol. 57, no. 16, pp. 2810-2815, 1991.

[6] L. de Figueiredo Vilela, V. Mattos de Mello, V.C. Branco Reis, E.P. da Silva Bon, F.A. Gonçalves Torres, B. Cruz Neves, et al. “Functional expression of *Burkholderia cenocepacia* xylose isomerase in yeast increases etanol production from glucose-xylose blend.” Bioresource Techonogy, vol. 128, pp. 792-796, 2013.

[7] Q.K. Beg, M. Kapoor, L. Mahajan, G.S. Hoondal. “Microbial xylanases and their industrial applications: A review.” Applied Microbiology and Biotechnology, vol. 56, no. 3-4, pp326-328, 2001.

[8] B.L. Cooper Bribiesca. “Enzimas xilanolíticas bacterianas y sus aplicaciones industriales. [Bacterial xylanolytic enzymes and their industrial applications.]” © VERTIENTES Revista Especializada en Ciencias de la Salud, vol. 16, no. 1, pp. 19-22, 2013.

Growing *Chlorella sorokiniana* heterotrophically, with sodium bicarbonate as a source of carbon

Pérez Nolasco Nathalia[1], Dávila Catalina, PhD[2], Department of Biology, School of Natural Sciences and Technology
Universidad del Turabo, Gurabo, PR, 00937 nperez175@gmail.com davilac2@suagm.edu

Abstract **Microalgae are promising candidates for biofuels production, given their capability of accumulating high proportions of oil. Furthermore, several subproducts can be generated from microalgae cultures, such as bioplastics, nutraceuticals, and animal feed, among others. However, when carbon dioxide is utilized as the sole source of carbon, biomass production is low. Finding a methodology for reaching high biomass values in shorter time would overcome this limitation. Among the alternatives that have been proposed for an accelerated microalgal growth is the addition of sodium bicarbonate. In this study, Chlorella sorokiniana, a freshwater microalga, was cultured in the presence of different concentrations of sodium bicarbonate in triplicate. pH was monitored daily and adjusted if necessary. Biomass was assessed by counting cells every two days in a hemocytometer.**

Keywords—microalgae, mixotrophic metabolism, sodium bicarbonate

I. Introduction

Many microalgae strains can grow mixotrophically, i.e. with CO2 as the sole source of carbon when light is present and utilizing other sources of carbon, both inorganic and organic, in the absence of light [1], [2]. Through mixotrophic metabolism, an accelerated growth can be achieved, which is desirable in large scale microalgae culture projects. Previous studies have found higher biomass production and growth rates when growing microalgae with sodium bicarbonate (NaHCO3) as the sole source of carbon [3], [4]. The aim of this work was to study the effect of sodium bicarbonate supplementation in biomass production of *Chlorella sorokiniana*. We added NaHCO3 at three different concentrations in triplicate and compare cell numbers with a control group. Determining the effectiveness of NaHCO3 addition could set the basis for attaining high biomass values in shorter times, and thus, for lowering production costs.

II. MATERIALS AND METHODS

Proteose culture medium was prepared, following instructions in [5]. Sodium bicarbonate was added to the culture medium in three different concentrations (2 g/L, 10 g/L, and 20 g/L) and in triplicate. Also, as a control group Proteose media without added NaHCO3 was used. In each replicate, an inoculum of 3.5×10^3 cells/mL (final concentration) was inoculated. Flasks were incubated under constant light and agitation to prevent cell precipitation for 2 weeks. Cell growth was monitored every two days by counting cells with a hemocytometer. During the incubation time, pH was controlled daily and adjusted with phosphoric acid (H_3PO_4) if necessary.

III. RESULTS AND DISCUSSION

A significant increase in growth was observed in the flasks containing 10 g/L $NaHCO_3$. Even though there was a difference in cell counts for each concentration, the three treatments had lower cell numbers than the control, indicating that sodium bicarbonate supplementation did not increase algal growth, as expected (figure 1). These results could be caused by environmental contaminants competing with the microalgae and by small predators observed in our cultures. Another key factor affecting algal growth is the pH. C. sorokiniana needs a pH of 7-9 for optimal growth and any deviations to this values can cause the microalgae to die. Although pH was measured daily and adjusted by adding H_3PO_4, the constant fluctuation in pH values could had a negative effect in algal growth.

Although increased biomass values were not achieved, efforts in finding suitable sources of carbon for growing microalgae heterotrophically should continue. This can translate in both economic and environmental benefits in large scale algae culture projects. Also, studies on the suitability of $NaHCO_3$ supplementation must be conducted with other microalgae strains.

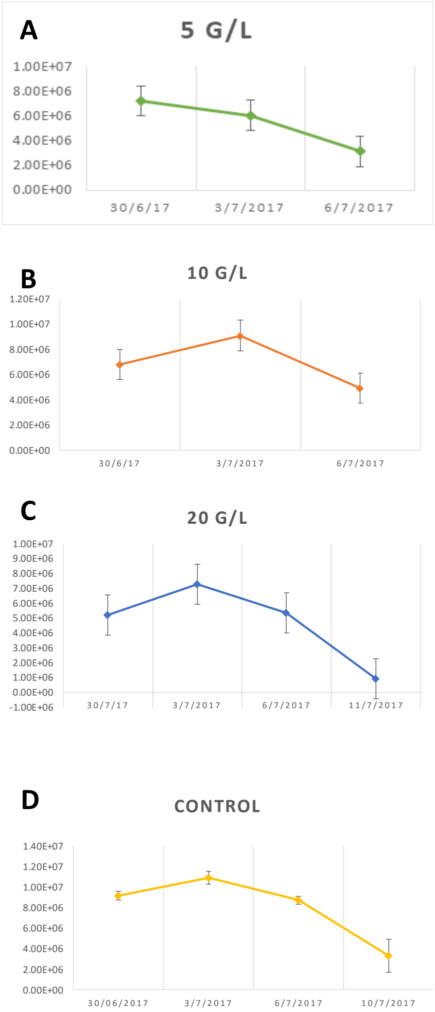

Fig. 1. Growth of C. sorokiniana (cells/mL) under four different $NaHCO_3$ concentrations

ACKNOWLEDGMENT

This project was supported by the Puerto Rico Energy Center (PREC), School of Engineer, Universidad del Turabo.

REFERENCES

[1] Ortiz-Moreno, Martha L., Caroll E. Cortés-Castillo, Julián Sánchez-Villarraga, Jorge Padilla, “Evaluación del crecimiento de la microalga Chlorella sorokiniana en diferentes medios de cultivo en condiciones autotróficas y mixotróficas.,” *Orinoquia*, vol. 16, no. 1, 2012.

[2] Bermúdez, José Luis, Gloria Sánchez, Gisela Fuenmayor, “Efecto de la fuente de carbono sobre el crecimiento y producción de pigmentos de la microalga marina Chroomonas sp.,” *Ciencia*, vol. 11, no. 4, 2003.

[3] White, D. A., A. Pagarette, P. Rooks, “The effect of sodium bicarbonate supplementation on growth and biochemical composition of marine microalgae cultures.,” *J. Appl. Phycol.*, vol. 25, no. 1, pp. 153–165, 2013.

[4] G. S. Keyuri Mokashi, Vishaka Shetty, Sangeetha Annie George, “Sodium Bicarbonate as Inorganic Carbon Source for Higher Biomass and Lipid Production Integrated Carbon Capture in Chlorella vulgaris.,” *Achiev. Life Sci.*, vol. 10, no. 1, pp. 111–117, 2016.

[5] University of Texas at Austin, “Utex Culture Collection of Algae.” [Online]. Available: https://utex.org/.

Amaury Malavé, PhD
School of Engineering
Universidad del Turabo, Gurabo, PR, USA

Catalina Dávila, PhD
School of Natural Science and Technology
Universidad del Turabo, Gurabo, PR, USA

Diego Aponte, MSEE
School of Engineering
Universidad del Turabo, Gurabo, PR, USA

Idalides Vergara, PhD
School of Engineering
Universidad del Turabo, Gurabo, PR, USA

Ileana González, PhD
School of Natural Science and Technology
Universidad del Turabo, Gurabo, PR, USA

José Maeso, MSEE
School of Engineering
Universidad del Turabo, Gurabo, PR, USA

José Perez Jimenez, PhD
School of Natural Science and Technology
Universidad del Turabo, Gurabo, PR, USA

Luz Torres, PhD
School of Engineering
Universidad del Turabo, Gurabo, PR, USA

Faculty

Paulette González
School of Natural Science and Technology
Universidad del Turabo, Gurabo, PR, USA

Harim Delgado
School of Natural Science and Technology
Universidad del Turabo, Gurabo, PR, USA

Luis Benítez
School of Engineering
Universidad del Turabo, Gurabo, PR, USA

Juan Rivera
School of Engineering
Universidad del Turabo, Gurabo, PR, USA

Pedro De Jesús
School of Engineering
Universidad del Turabo, Gurabo, PR, USA

Fernando Arroyo
School of Engineering
Universidad del Turabo, Gurabo, PR, USA

Ian Maldonado
School of Engineering
Universidad del Turabo, Gurabo, PR, USA

Jhonatan Carbajal
School of Engineering
Universidad del Turabo, Gurabo, PR, USA

Kenneth Mckenzie
School of Engineering
Universidad del Turabo, Gurabo, PR, USA

Carl Camis
Engineering
American University, Bayamón, PR, USA

Lewis Díaz
School of Natural Science and Technology
Universidad del Turabo, Gurabo, PR, USA

Oscar Faura
School of Engineering
Universidad del Turabo, Gurabo, PR, USA

Xavier Lopez
School of Engineering
Universidad del Turabo, Gurabo, PR, USA

Abel Concepción
School of Engineering
Universidad del Turabo, Gurabo,

Edwin G Velázquez Perez
School of Natural Science and Technology
Universidad del Turabo, Gurabo, PR, USA

Jonathan López
School of Natural Science and Technology
Universidad del Turabo, Gurabo, PR, USA

Janmary Colón
School of Natural Science and Technology
Universidad del Turabo, Gurabo, PR, USA

Nathalia Pérez
School of Natural Science and Techology
Universidad del Turabo, Gurabo, PR, USA

Students

UNIVERSIDAD
DEL TURABO
SISTEMA UNIVERSITARIO
ANA G. MÉNDEZ